PLANE WAVE DIFFRACTION BY A FINITE PARALLEL-PLATE WAVEGUIDE WITH FOUR-LAYER MATERIAL LOADING: PART 1 — THE CASE OF E POLARIZATION

J. P. Zheng and K. Kobayashi

Department of Electrical, Electronic, and Communication
Engineering
Chuo University
Tokyo 112-8551, Japan

Abstract—The plane wave diffraction by a finite parallel-plate waveguide with four-layer material loading is rigorously analyzed for the case of E polarization using the Wiener-Hopf technique. Introducing the Fourier transform for the scattered field and applying boundary conditions in the transform domain, the problem is formulated in terms of the simultaneous Wiener-Hopf equations, which are solved via the factorization and decomposition procedure together with a rigorous asymptotics. The scattered field is evaluated explicitly by taking the inverse Fourier transform and applying the saddle point method. Representative numerical examples of the radar cross section (RCS) are shown for various physical parameters and the far field scattering characteristics are discussed in detail.

1. INTRODUCTION

The analysis of electromagnetic wave scattering by open-ended metallic waveguide cavities is an important subject in the prediction and reduction of the radar cross section (RCS) of a target [1–6]. This problem serves as a simple model of duct structures such as jet engine intakes of aircrafts and cracks occurring on surfaces of general complicated bodies. Some of the diffraction problems involving two- and three-dimensional (2-D and 3-D) cavities have been analyzed thus far based on high-frequency techniques and numerical methods [7–13]. It appears, however, that the solutions due to these approaches are not uniformly valid for arbitrary dimensions of the cavity. Therefore it is

desirable to overcome the disadvantages of the previous works to obtain solutions which are uniformly valid in arbitrary cavity dimensions.

The Wiener-Hopf technique [14–16] is one of the powerful approaches for analyzing wave scattering and diffraction problems involving canonical geometries, which is mathematically rigorous in the sense that the edge condition, required for the uniqueness of the solution, is explicitly incorporated into the analysis. There are some papers treating cavity diffraction problems based on the Wiener-Hopf technique [17, 18], where efficient approximate solutions have been obtained. In the previous papers [19–23], we have considered several 2-D cavities formed by semi-infinite and finite parallel-plate waveguides, and analyzed the plane wave diffraction rigorously by using the Wiener-Hopf technique. In addition, we have considered in [24, 25] a finite parallel-plate waveguide with three-layer material loading as a geometry that can form cavities, and carried out the Wiener-Hopf analysis of the plane wave diffraction. As a result, it has been verified that our final solutions are valid for broad frequency range and can be used as reference solutions.

In this two-part paper, we shall consider a finite parallel-plate waveguide with four-layer material loading as an important generalization to the geometry in [24, 25], and analyze the plane wave diffraction for both E and H polarizations. It should be noted that, due to the existence of an additional material layer, the Wiener-Hopf analysis becomes considerably complicated in comparison to our previous analysis for the three-layer case [24, 25]. The case of E polarization is considered in this first part, whereas the analysis for the H-polarized case will be presented in the second part [26].

First in Section 2, the Fourier transform for the unknown scattered field is introduced and the transformed wave equations are derived by taking the Fourier transform of the 2-D Helmholtz equation, which contain unknown inhomogeneous terms occurring due to medium discontinuities along the transform axis. Section 3 discusses the formulation of the problem. The transformed wave equations are solved by expanding the inhomogeneous terms into the Fourier sine series and a scattered field representation in the transform domain is derived. Subsequently by using boundary conditions in the transform domain, the problem is formulated in terms of the simultaneous Wiener-Hopf equations satisfied by the unknown spectral functions, where the unknown Fourier expansion coefficients are also involved. There are some important relations between the Fourier coefficients and the unknown functions, which will be investigated in Appendix. In Section 4, the Wiener-Hopf equations are solved exactly via the factorization and decomposition procedure leading to

the formal solution. The solution, however, involves infinite branch-cut integrals with unknown integrands as well as infinite series with unknown coefficients. In Section 5, we shall develop an efficient method for evaluating the branch-cut integrals asymptotically and determining the unknown coefficients approximately, and derive an approximate solution to the Wiener-Hopf equations, which involves numerical inversion of matrix equations. It should be noted that our final approximate solution is valid for the waveguide length greater than the incident wavelength. Subsequently in Section 6, the scattered field inside and outside the waveguide is evaluated explicitly by taking the Fourier inverse of the solution in the transform domain. The field inside the waveguide is expressed in terms of the *TE* mode series, whereas for the field outside the waveguide, a far field asymptotic expression is derived using the saddle point method. In Section 7, we shall present illustrative numerical examples of the RCS for various physical parameters, and discuss the far field scattering characteristics of the waveguide in detail. Section 8 contains some concluding remarks.

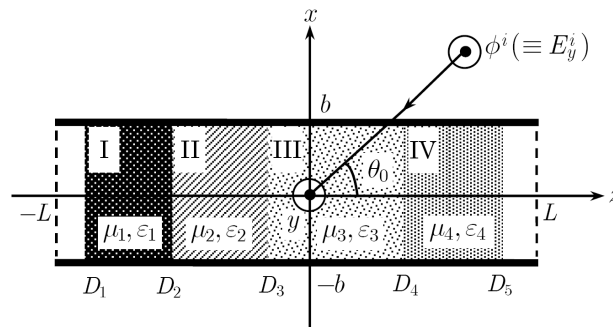The time factor is assumed to be $e^{-i\omega t}$ and suppressed throughout this paper.

Figure 1. Geometry of the problem.

2. TRANSFORMED WAVE EQUATIONS

We consider the diffraction of an E-polarized plane wave by a finite parallel-plate waveguide with four-layer material loading as shown in Fig. 1, where $-L < D_1 < D_2 < D_3 < D_4 < D_5 < L$ and the E polarization implies that the incident electric field is parallel to the y-axis. The waveguide plates are perfectly conducting and of zero thickness, and the material layers I $(D_1 < z < D_2)$, II $(D_2 < z < D_3)$, III $(D_3 < z < D_4)$, and IV $(D_4 < z < D_5)$ are characterized by the relative permittivity ε_m and the relative permeability μ_m for

$m = 1, 2, 3$, and 4, respectively. In view of the geometry and the characteristics of the incident field, this is a 2-D problem.

Define the total electric field $\phi^t(x, z)[\equiv E_y^t(x, z)]$ by

$$\phi^t(x, z) = \phi^i(x, z) + \phi(x, z), \tag{1}$$

where $\phi^i(x, z)$ is the incident field given by

$$\phi^i(x, z) = e^{-ik(x \sin \theta_0 + z \cos \theta_0)} \tag{2}$$

for $0 < \theta_0 < \pi/2$ with $k \left[\equiv \omega(\varepsilon_0 \mu_0)^{1/2}\right]$ being the free-space wavenumber. The total field $\phi^t(x, z)$ satisfies the 2-D Helmholtz equation

$$\left[\partial^2/\partial x^2 + \partial^2/\partial z^2 + \mu(x, z)\varepsilon(x, z)k^2\right] \phi^t(x, z) = 0, \tag{3}$$

where

$$\mu(x, z) = \begin{cases} \mu_1(\text{layer I}) \\ \mu_2(\text{layer II}) \\ \mu_3(\text{layer III}) \\ \mu_4(\text{layer IV}) \\ 1(\text{otherwise}) \end{cases}, \quad \varepsilon(x, z) = \begin{cases} \varepsilon_1(\text{layer I}) \\ \varepsilon_2(\text{layer II}) \\ \varepsilon_3(\text{layer III}) \\ \varepsilon_4(\text{layer IV}) \\ 1(\text{otherwise}) \end{cases}. \tag{4}$$

Nonzero components of the total electromagnetic fields are derived from

$$\left(E_y^t, H_x^t, H_z^t\right) = \left[\phi^t, \frac{i}{\omega\mu_0\mu(x, z)} \frac{\partial \phi^t}{\partial z}, \frac{i}{\omega\mu_0\mu(x, z)} \frac{\partial \phi^t}{\partial x}\right]. \tag{5}$$

We assume that the vacuum is slightly lossy as in $k = k_1 + ik_2$ with $0 < k_2 \ll k_1$. The solution for real k is obtained by letting $k_2 \to +0$ at the end of analysis. It follows from the radiation condition that the scattered field satisfies

$$\phi(x, z) = O\left(e^{-k_2|z| \cos \theta_0}\right) \tag{6}$$

as $|z| \to \infty$. We now define the Fourier transform of the scattered field $\phi(x, z)$ with respect to z as

$$\Phi(x, \alpha) = (2\pi)^{-1/2} \int_{-\infty}^{\infty} \phi(x, z)e^{i\alpha z} dz, \tag{7}$$

where $\alpha = \text{Re}\alpha + i\text{Im}\alpha (\equiv \sigma + i\tau)$. In view of the radiation condition, it is found that $\Phi(x, \alpha)$ is regular in the strip $|\tau| < k_2 \cos \theta_0$ of the

complex α-plane. For convenience of analysis, we also introduce the Fourier integrals as

$$\Phi_{\pm}(x,\,\alpha) = \pm(2\pi)^{-1/2}\int_{\pm L}^{\pm\infty}\phi(x,\,z)e^{i\alpha(z\mp L)}dz, \tag{8}$$

$$\Phi_m(x,\,\alpha) = \begin{cases} (2\pi)^{-1/2}\displaystyle\int_{-L}^{D_1}\phi^t(x,\,z)e^{i\alpha z}dz, \ m = 1, \\[2mm] (2\pi)^{-1/2}\displaystyle\int_{D_{m-1}}^{D_m}\phi^t(x,\,z)e^{i\alpha z}dz, \ m = 2,\,3,\,4,\,5, \\[2mm] (2\pi)^{-1/2}\displaystyle\int_{D_5}^{L}\phi^t(x,\,z)e^{i\alpha z}dz, \ m = 6. \end{cases} \tag{9}$$

It is verified from the theory of Fourier integrals that $\Phi_+(x,\,\alpha)$ and $\Phi_-(x,\,\alpha)$ are regular in the upper half-plane $\tau > -k_2\cos\theta_0$ and the lower half-plane $\tau < k_2\cos\theta_0$, respectively, whereas $\Phi_m(x,\,\alpha)$ for $m = 1,\,2,\,3,\,\ldots,\,6$ are entire functions. By using (8) and (9), we can express $\Phi(x,\,\alpha)$ as

$$\Phi(x,\,\alpha) = \Psi(x,\,\alpha) + \Phi_{(1)}(x,\,\alpha), \tag{10}$$

where

$$\Psi(x,\,\alpha) = e^{-i\alpha L}\Psi_-(x,\,\alpha) + e^{i\alpha L}\Psi_{(+)}(x,\,\alpha), \tag{11}$$

$$\Phi_{(1)}(x,\,\alpha) = \sum_{m=1}^{6}\Phi_m(x,\,\alpha) \tag{12}$$

with

$$\Psi_-(x,\,\alpha) = \Phi_-(x,\,\alpha) + A\frac{e^{-ikx\sin\theta_0}}{\alpha - k\cos\theta_0}, \tag{13}$$

$$\Psi_{(+)}(x,\,\alpha) = \Phi_+(x,\,\alpha) - B\frac{e^{-ikx\sin\theta_0}}{\alpha - k\cos\theta_0}, \tag{14}$$

$$A = \frac{e^{ikL\cos\theta_0}}{(2\pi)^{1/2}i}, \quad B = \frac{e^{-ikL\cos\theta_0}}{(2\pi)^{1/2}i}. \tag{15}$$

The parentheses in the subscript of $\Psi_{(+)}(x,\,\alpha)$ imply that $\Psi_{(+)}(x,\,\alpha)$ is regular in $\tau > -k_2\cos\theta_0$ except for a simple pole at $\alpha = k\cos\theta_0$.

In order to derive transformed wave equations, we note that

$$\left(\partial^2/\partial x^2 + \partial^2/\partial z^2 + k^2\right)\phi(x,\,z) = 0 \tag{16}$$

and

$$\left(\partial^2/\partial x^2 + \partial^2/\partial z^2 + K_m^2\right)\phi^t(x,\,z) = 0 \tag{17}$$

hold for unloaded and loaded regions, respectively, where $K_m = (\mu_m \varepsilon_m)^{1/2} k$ for $m = 1,\, 2,\, 3,\, 4$. For the region $|x| > b$, we can show by taking the Fourier transform of (16) and using (6) that

$$\left(d^2/dx^2 - \gamma^2\right)\Phi(x,\,z) = 0 \tag{18}$$

holds for any α in the strip $|\tau| < k_2 \cos\theta_0$, where $\gamma = (\alpha^2 - k^2)^{1/2}$ with $\mathrm{Re}\gamma > 0$. Equation (18) is the transformed wave equation for the region $|x| > b$.

The derivation of transformed wave equations for the region $|x| < b$ is involved, since there are medium discontinuities across the surfaces at $z = D_1,\, D_2,\, D_3,\, D_4,\, D_5$. We now multiply both sides of (17) by $(2\pi)^{-1/2} e^{i\alpha z}$ and integrate with respect to z over the ranges $-\infty < z < D_1$ and $D_5 < z < \infty$. Taking into account the boundary conditions for tangential electromagnetic fields at $z = D_1,\, D_5$, we derive by some manipulations that

$$\left(d^2/dx^2 - \gamma^2\right)\left[\Phi_1(x,\,\alpha) + e^{-i\alpha L}\Psi_-(x,\,\alpha)\right] = -e^{i\alpha D_1}\mu_1^{-1}f_1(x) - i\alpha g_1(x) \tag{19}$$

for $\tau < k_2 \cos\theta_0$, and that

$$\left(d^2/dx^2 - \gamma^2\right)\left[\Phi_6(x,\,\alpha) + e^{-i\alpha L}\Psi_{(+)}(x,\,\alpha)\right] = e^{i\alpha D_5}\left[\mu_4^{-1}f_5(x) - i\alpha g_5(x)\right] \tag{20}$$

for $\tau > -k_2 \cos\theta_0$ with $\alpha \neq k \cos\theta_0$, where

$$f_1(x) = (2\pi)^{-1/2}\frac{\partial\phi^t(x,\,D_1+0)}{\partial z}, \tag{21}$$

$$g_1(x) = (2\pi)^{-1/2}\phi^t(x,\,D_1), \tag{22}$$

$$f_5(x) = (2\pi)^{-1/2}\frac{\partial\phi^t(x,\,D_5-0)}{\partial z}, \tag{23}$$

$$g_5(x) = (2\pi)^{-1/2}\phi^t(x,\,D_5). \tag{24}$$

Next we multiply both sides of (17) by $(2\pi)^{-1/2} e^{i\alpha z}$ and integrate with respect to z for $D_1 < z < D_2$, $D_2 < z < D_3$, $D_3 < z < D_4$, and $D_4 < z < D_5$. This gives, after utilizing the boundary conditions for tangential electromagnetic fields at $z = D_1,\, D_2,\, D_3,\, D_4,\, D_5$,

$$\left(d^2/dx^2 - \Gamma_1^2\right)\Phi_2(x,\,\alpha)$$
$$= e^{i\alpha D_1}\left[f_1(x) - i\alpha g_1(x)\right] - e^{i\alpha D_2}\left[(\mu_1/\mu_2)f_2(x) - i\alpha g_2(x)\right], \tag{25}$$

$$\left(d^2/dx^2 - \Gamma_2^2\right) \Phi_3(x, \alpha)$$
$$= e^{i\alpha D_2} \left[f_2(x) - i\alpha g_2(x)\right] - e^{i\alpha D_3} \left[f_3(x) - i\alpha g_3(x)\right], \qquad (26)$$

$$\left(d^2/dx^2 - \Gamma_3^2\right) \Phi_4(x, \alpha)$$
$$= e^{i\alpha D_3} \left[(\mu_3/\mu_2) f_3(x) - i\alpha g_3(x)\right] - e^{i\alpha D_4} \left[f_4(x) - i\alpha g_4(x)\right], \quad (27)$$

$$\left(d^2/dx^2 - \Gamma_4^2\right) \Phi_5(x, \alpha)$$
$$= e^{i\alpha D_4} \left[f_4(x) - i\alpha g_4(x)\right] - e^{i\alpha D_5} \left[f_5(x) - i\alpha g_5(x)\right], \qquad (28)$$

where $\Gamma_m = (\alpha^2 - K_m^2)^{1/2}$ with $\mathrm{Re}\,\Gamma_m > 0$ and

$$f_m(x) = (2\pi)^{-1/2} \frac{\partial \phi^t(x, D_m + 0)}{\partial z}, \qquad (29)$$

$$g_m(x) = (2\pi)^{-1/2} \phi^t(x, D_m) \qquad (30)$$

for $m = 2, 3, 4$. Equations (19), (20), and (25)–(28) are the transformed wave equations for the region $|x| < b$.

3. SIMULTANEOUS WIENER-HOPF EQUATIONS

First we shall solve the transformed wave Equations (18)–(20) and (25)–(28) to derive a scattered field representation in the Fourier transform domain. Using the boundary conditions for tangential electric fields across $x = \pm b$, the solution of (18) is expressed as

$$\Phi(x, \alpha) = \Phi(b, \alpha)e^{-\gamma(x-b)}, \quad x \geq b,$$
$$= \Phi(-b, \alpha)e^{\gamma(x+b)}, \quad x \leq -b, \qquad (31)$$

where we have used the following boundary conditions for tangential electric fields across $x = \pm b$:

$$\Phi_{\pm} (\pm b + 0, \alpha) = \Phi_{\pm} (\pm b - 0, \alpha) \equiv \Phi_{\pm} (\pm b, \alpha), \qquad (32)$$
$$\Phi_m (\pm b + 0, \alpha) = \Phi_m (\pm b - 0, \alpha) = 0, \ m = 1, 2, 3, \ldots, 6. \quad (33)$$

Equation (31) gives the scattered field representation for $|x| > b$.

The derivation of a field representation for the region $|x| < b$ is complicated since the transformed wave equations involve the unknown inhomogeneous terms $f_m(x)$ and $g_m(x)$ for $m = 1, 2, 3, 4, 5$. We expand these terms using the Fourier sine series as in

$$f_m(x) = \frac{1}{b} \sum_{n=1}^{\infty} f_{mn} \sin \frac{n\pi}{2b}(x + b), \qquad (34)$$

$$g_m(x) = \frac{1}{b} \sum_{n=1}^{\infty} g_{mn} \sin \frac{n\pi}{2b}(x + b) \tag{35}$$

for $|x| < b$, where

$$f_{mn} = \int_{-b}^{b} f_m(x) \sin \frac{n\pi}{2b}(x + b)dx, \tag{36}$$

$$g_{mn} = \int_{-b}^{b} g_m(x) \sin \frac{n\pi}{2b}(x + b)dx. \tag{37}$$

The Fourier coefficients f_{mn} and g_{mn} for $m = 1$, 2, 3, 4, 5 have various analytical properties which play a significant role in the subsequent analysis. These properties are discussed in detail in Appendix. Taking into account (34) and (35) and following a procedure similar to that employed in [20], we derive the solutions of (19), (20), and (25)–(28) with the result that

$$
\begin{aligned}
&\Phi_1(x,\,\alpha) + e^{-i\alpha L}\Psi_-(x,\,\alpha) \\
&= e^{-i\alpha L}\left[\Psi_-(b,\,\alpha)\frac{\sinh\gamma(x+b)}{\sinh 2\gamma b} - \Psi_-(-b,\,\alpha)\frac{\sinh\gamma(x-b)}{\sinh 2\gamma b}\right] \\
&\quad + \frac{e^{i\alpha D_1}}{b}\sum_{n=1}^{\infty}\frac{c_{1n}^-(\alpha)}{\alpha^2 + \gamma_n^2}\sin\frac{n\pi}{2b}(x+b),
\end{aligned}
\tag{38}
$$

$$
\begin{aligned}
&\Phi_6(x,\,\alpha) + e^{i\alpha L}\Psi_{(+)}(x,\,\alpha) \\
&= e^{i\alpha L}\left[\Psi_{(+)}(b,\,\alpha)\frac{\sinh\gamma(x+b)}{\sinh 2\gamma b} - \Psi_{(+)}(-b,\,\alpha)\frac{\sinh\gamma(x-b)}{\sinh 2\gamma b}\right] \\
&\quad - \frac{e^{i\alpha D_5}}{b}\sum_{n=1}^{\infty}\frac{c_{5n}^-(\alpha)}{\alpha^2 + \gamma_n^2}\sin\frac{n\pi}{2b}(x+b),
\end{aligned}
\tag{39}
$$

$$
\Phi_m(x,\,\alpha) = -\frac{1}{b}\sum_{n=1}^{\infty}\frac{e^{i\alpha D_{m-1}}c_{m-1,\,n}^+(\alpha) - e^{i\alpha D_m}c_{mn}^-(\alpha)}{\alpha^2 + \Gamma_{m-1,\,n}^2}\sin\frac{n\pi}{2b}(x+b)
$$
$$
\text{for} \quad m = 2,\,3,\,4,\,5, \tag{40}
$$

where

$$\gamma_n = \left[(n\pi/2b)^2 - k^2\right]^{1/2} \text{ for } n \geq 1, \tag{41}$$

$$\Gamma_{mn} = \left[(n\pi/2b)^2 - K_m^2\right]^{1/2} \text{ for } n \geq 1,\, m = 1,\,2,\,3,\,4, \tag{42}$$

$$c_{1n}^-(\alpha) = \mu_1^{-1}f_{1n} - i\alpha g_{1n},\, c_{1n}^+(\alpha) = f_{1n} - i\alpha g_{1n}, \tag{43}$$

$$c_{2n}^-(\alpha) = (\mu_1/\mu_2)f_{2n} - i\alpha g_{2n}, \ c_{2n}^+(\alpha) = f_{2n} - i\alpha g_{2n}, \tag{44}$$

$$c_{3n}^-(\alpha) = f_{3n} - i\alpha g_{3n}, \ c_{3n}^+(\alpha) = (\mu_3/\mu_2)f_{3n} - i\alpha g_{3n}, \tag{45}$$

$$c_{4n}^+(\alpha) = f_{4n} - i\alpha g_{4n}, \ c_{4n}^-(\alpha) = f_{4n} - i\alpha g_{4n}, \tag{46}$$

$$c_{5n}^-(\alpha) = f_{5n} - i\alpha g_{5n}, \ c_{5n}^+(\alpha) = \mu_4^{-1}f_{5n} - i\alpha g_{5n}. \tag{47}$$

Substituting (38)–(40) into (10), the scattered field representation for the region $|x| < b$ is derived.

Summarizing the above results, an explicit expression of $\Phi(x, \alpha)$ is found to be

$$\Phi(x, \alpha) = \Psi(\pm b, \alpha)e^{\mp\gamma(x\mp b)} \ \text{ for } \ x \gtrless \pm b,$$

$$= \Psi(b, \alpha)\frac{\sinh\gamma(x+b)}{\sinh 2\gamma b} - \Psi(-b, \alpha)\frac{\sinh\gamma(x-b)}{\sinh 2\gamma b}$$

$$-\frac{1}{b}\sum_{n=1}^{\infty}\frac{e^{i\alpha D_5}c_{5n}^+(\alpha) - e^{i\alpha D_1}c_{1n}^-(\alpha)}{\alpha^2 + \gamma_n^2}\sin\frac{n\pi}{2b}(x+b)$$

$$-\frac{1}{b}\sum_{m=1}^{4}\sum_{n=1}^{\infty}\frac{e^{i\alpha D_m}c_{mm}^+(\alpha) - e^{i\alpha D_{m+1}}c_{m+1, n}^-(\alpha)}{\alpha^2 + \Gamma_{mn}^2}\sin\frac{n\pi}{2b}(x+b)$$

$$\text{for} \quad |x| < b. \tag{48}$$

Equation (48) is the scattered field representation in the Fourier transform domain and holds in the strip $|\tau| < k_2\cos\theta_0$.

Differentiating the field representation in (48) for $x \gtrless \pm b$ with respect to x and setting $x = \pm b \pm 0$, we obtain that

$$\Phi'(b+0, \alpha) = -\gamma\Psi(-b, \alpha), \tag{49}$$

$$\Phi'(-b-0, \alpha) = -\gamma\Psi(-b, \alpha), \tag{50}$$

where the prime denotes differentiation with respect to x. We also differentiate the field representation for $|x| < b$ in (48) and set $x = \pm b \mp 0$ in the results. Then it follows that

$$\Phi'(b-0, \alpha) = \gamma\Psi(b, \alpha)\coth 2\gamma b - \gamma\Psi(-b, \alpha)\operatorname{csch}2\gamma b$$

$$-\frac{1}{b}\sum_{n=1}^{\infty}(-1)^n\frac{n\pi}{2b}\frac{e^{i\alpha D_5}c_{5n}^+(\alpha) - e^{i\alpha D_1}c_{1n}^-(\alpha)}{\alpha^2 + \gamma_n^2}$$

$$-\frac{1}{b}\sum_{m=1}^{4}\sum_{n=1}^{\infty}(-1)^n\frac{n\pi}{2b}\frac{e^{i\alpha D_m}c_{mn}^+(\alpha) - e^{i\alpha D_{m+1}}c_{m+1, n}^-(\alpha)}{\alpha^2 + \Gamma_{mn}^2}, \tag{51}$$

$$\Phi'(-b+0,\alpha){=}\gamma\Psi(b,\alpha)\operatorname{csch}2\gamma b-\gamma\Psi(-b,\alpha)\coth 2\gamma b$$

$$-\frac{1}{b}\sum_{n=1}^{\infty}\frac{n\pi}{2b}\frac{e^{i\alpha D_5}c_{5n}^+(\alpha)-e^{-i\alpha D_1}c_{1n}^-(\alpha)}{\alpha^2+\gamma_n^2}$$

$$-\frac{1}{b}\sum_{m=1}^{4}\sum_{n=1}^{\infty}\frac{n\pi}{2b}\frac{e^{i\alpha D_m}c_{mn}^+(\alpha)-e^{i\alpha D_{m+1}}c_{m+1,n}^-(\alpha)}{\alpha^2+\Gamma_{mn}^2}. \quad (52)$$

Subtracting (51) and (52) from (49) and (50), respectively and taking the sum and difference of the resultant equations, we obtain, after some manipulations, that

$$J_1^d(\alpha) = -\frac{e^{-i\alpha L}U_-(\alpha)+e^{i\alpha L}U_{(+)}(\alpha)}{M(\alpha)}$$

$$-\sum_{n=1,\,\text{odd}}^{\infty}\frac{n\pi}{b^2}\left[\frac{e^{i\alpha D_5}c_{5n}^+(\alpha)-e^{i\alpha D_1}c_{1n}^-(\alpha)}{\alpha^2+\gamma_n^2}\right.$$

$$\left.+\sum_{m=1}^{4}\frac{e^{i\alpha D_m}c_{mn}^+(\alpha)-e^{i\alpha D_{m+1}}c_{m+1,\,n}^-(\alpha)}{\alpha^2+\Gamma_{mn}^2}\right], \quad (53)$$

$$J_1^s(\alpha) = -\frac{e^{-i\alpha L}V_-(\alpha)+e^{i\alpha L}V_{(+)}(\alpha)}{N(\alpha)}$$

$$+\sum_{n=2,\,\text{even}}^{\infty}\frac{n\pi}{b^2}\left[\frac{e^{i\alpha D_5}c_{5n}^+(\alpha)-e^{i\alpha D_1}c_{1n}^-(\alpha)}{\alpha^2+\gamma_n^2}\right.$$

$$\left.+\sum_{m=1}^{4}\frac{e^{i\alpha D_m}c_{mn}^+(\alpha)-e^{i\alpha D_{m+1}}c_{m+1,n}^-(\alpha)}{\alpha^2+\Gamma_{mn}^2}\right] \quad (54)$$

for $|\tau| < k_2\cos\theta_0$, where

$$U_-(\alpha) = \Psi_-(b,\alpha)+\Psi_-(-b,\alpha), \quad (55)$$
$$U_{(+)}(\alpha) = \Psi_{(+)}(b,\alpha)+\Psi_{(+)}(-b,\alpha), \quad (56)$$
$$V_-(\alpha) = \Psi_-(b,\alpha)-\Psi_-(-b,\alpha), \quad (57)$$
$$V_{(+)}(\alpha) = \Psi_{(+)}(b,\alpha)-\Psi_{(+)}(-b,\alpha), \quad (58)$$
$$J_1^{d,\,s}(\alpha) = J_1(b,\alpha)\mp J_1(-b,\alpha), \quad (59)$$
$$J_1(\pm b,\alpha) = \Phi'_{(1)}(\pm b\pm 0,\alpha)-\Phi'_{(1)}(\pm b\mp 0,\alpha), \quad (60)$$
$$M(\alpha) = \frac{e^{-\gamma b}\cosh\gamma b}{\gamma}, \ N(\alpha)=\frac{e^{-\gamma b}\sinh\gamma b}{\gamma}. \quad (61)$$

Equations (53) and (54) are the simultaneous Wiener-Hopf equations satisfied by the unknown spectral functions, where the unknown Fourier coefficients are also involved.

4. FORMAL SOLUTION

The kernel functions $M(\alpha)$ and $N(\alpha)$ defined by (61) are factorized as [20]

$$M(\alpha) = M_+(\alpha)M_-(\alpha), \quad N(\alpha) = N_+(\alpha)N_-(\alpha), \qquad (62)$$

where $M_\pm(\alpha)$ and $N_\pm(\alpha)$ are the split functions given by

$$\begin{aligned}
&M_+(\alpha)[= M_-(-\alpha)] \\
=\ &(\cos kb)^{1/2} e^{i\pi/4}(k+\alpha)^{-1/2} \exp\left\{(i\gamma b/\pi)\ln[(\alpha-\gamma)/k]\right\} \\
&\cdot \exp\left\{(i\alpha b/\pi)[1 - C + \ln(\pi/2kb) + i\pi/2]\right\} \\
&\cdot \prod_{n=1,\,\mathrm{odd}}^{\infty}(1 + \alpha/i\gamma_n)e^{2i\alpha b/n\pi},
\end{aligned} \qquad (63)$$

$$\begin{aligned}
&N_+(\alpha)[= N_-(-\alpha)] \\
=\ &(\sin kb/k)^{1/2} \exp\left\{(i\gamma b/\pi)\ln[(\alpha-\gamma)/k]\right\} \\
&\cdot \exp\left\{(i\alpha b/\pi)[1 - C + \ln(2\pi/kb) + i\pi/2]\right\} \\
&\cdot \prod_{n=2,\,\mathrm{even}}^{\infty}(1 + \alpha/i\gamma_n)e^{2i\alpha b/n\pi}
\end{aligned} \qquad (64)$$

with $C\,(= 0.57721566\ldots)$ being Euler's constant. It is seem from (63) and (64) that $M_\pm(\alpha)$ and $N_\pm(\alpha)$ are regular and nonzero in $\tau \gtrless \mp k_2$. We can also verify that

$$M_\pm(\alpha) \sim (\mp 2i\alpha)^{-1/2}, \quad N_\pm(\alpha) \sim (\mp 2i\alpha)^{-1/2} \qquad (65)$$

as $\alpha \to \infty$ with $\tau \gtrless \mp k_2$. Taking into account the edge condition, we can show that the unknown functions in (53) and (54) behave asymptotically as

$$\left.\begin{aligned}
U_{(+)}(\alpha) \\
U_-(\alpha)
\end{aligned}\right\} = O\left(\alpha^{-3/2}\right),\ \tau \gtrless \mp k_2 \cos\theta_0, \qquad (66)$$

$$e^{\pm i\alpha L}J_1^d(\alpha) = O\left(\alpha^{-1/2}\right),\ \tau \gtrless 0 \qquad (67)$$

for $\alpha \rightarrow \infty$. We multiply both sides of (53) by $e^{\pm i\alpha L}M_{\pm}(\alpha)$ and decompose the results using (65)–(67). This leads to

$$
\frac{U_-(\alpha)}{M_-(\alpha)} - \frac{1}{2\pi i}\int_{C_2}\frac{e^{2i\beta L}U_{(+)}(\beta)}{M_-(\beta)(\beta-\alpha)}d\beta + \sum_{n=1,\,\text{odd}}^{\infty}\frac{n\pi}{2b}\frac{M_+(i\gamma_n)}{bi\gamma_n(\alpha-i\gamma_n)}
$$

$$
\cdot\left[e^{-\gamma_n(L+D_5)}c_{5n}^+(i\gamma_n) - e^{-\gamma_n(L+D_1)}c_{1n}^-(i\gamma_n)\right]
$$

$$
+\sum_{m=1}^{4}\sum_{n=1,\,\text{odd}}^{\infty}\frac{n\pi}{2b}\frac{M_+(i\Gamma_{mn})}{bi\Gamma_{mm}(\alpha-i\Gamma_{mn})}
$$

$$
\cdot\left[e^{-\Gamma_{mn}(L+D_1)}c_{mn}^+(i\Gamma_{mn}) - e^{-\Gamma_{mn}(L+D_{m+1})}c_{m+1,\,n}^-(i\Gamma_{mn})\right]=0,\;(68)
$$

$$
\frac{U_{(+)}(\alpha)}{M_+(\alpha)} + \frac{1}{2\pi i}\int_{C_1}\frac{e^{-2i\beta L}U_-(\beta)}{M_+(\beta)(\beta-\alpha)}d\beta
$$

$$
+\frac{2B\cos(kb\sin\theta_0)}{M_+(k\cos\theta_0)(\alpha-k\cos\theta_0)} - \sum_{n=1,\,\text{odd}}^{\infty}\frac{n\pi}{2b}\frac{M_+(i\gamma_n)}{bi\gamma_n(\alpha+i\gamma_n)}
$$

$$
\cdot\left[e^{-\gamma_n(L-D_5)}c_{5n}^+(-i\gamma_n) - e^{-\gamma_n(L-D_1)}c_{1n}^-(-i\gamma_n)\right]
$$

$$
-\sum_{m=1}^{4}\sum_{n=1,\,\text{odd}}^{\infty}\frac{n\pi}{2b}\frac{M_+(i\Gamma_{mn})}{bi\Gamma_{mn}(\alpha+i\Gamma_{mn})}
$$

$$
\cdot\left[e^{-\Gamma_{mn}(L-D_1)}c_{mn}^+(-i\Gamma_{mn}) - e^{-\Gamma_{mn}(L-D_{m+1})}c_{m+1,n}^-(-i\Gamma_{mn})\right]=0,\;(69)
$$

where C_1 and C_2 are the infinite integration paths running parallel to real axis in the β-plane, as shown in Fig. 2. Evaluating the integrals in (68) and (69) and arranging the results with the aid of (A4)–(A9) in Appendix, we derive that

$$
U_-(\alpha) = b^{1/2}M_-(\alpha)\left[\frac{A_u}{b(\alpha-k\cos\theta_0)} + \frac{J_u^{(1)}(\alpha)}{b^{1/2}}\right.
$$

$$
-\sum_{n=2}^{\infty}\frac{e^{-2\gamma_{2n-3}(L+D_1)}X_{2n-3}^-a_np_nu_n^-}{b(\alpha-i\gamma_{2n-3})}
$$

$$
\left. -\sum_{n=2}^{\infty}\frac{e^{-\gamma_{2n-3}(2L+D_1-D_5)}Y_{2n-3}^-a_np_nu_n^+}{b(\alpha-i\gamma_{2n-3})}\right],\qquad(70)
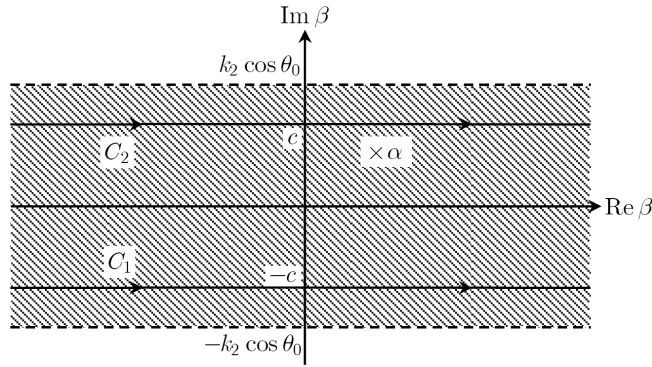$$

Figure 2. Integration paths C_1 and C_2 $(0 < |\tau| < c < k_2 \cos\theta_0)$.

$$
U_{(+)}(\alpha) = b^{1/2} M_+(\alpha) \left[-\frac{B_u}{b(\alpha - k\cos\theta_0)} + \frac{J_u^{(2)}(\alpha)}{b^{1/2}} \right.
$$

$$
+ \sum_{n=2}^{\infty} \frac{e^{-2\gamma_{2n-3}(L-D_5)} X_{2n-3}^+ a_n p_n u_n^+}{b(\alpha + i\gamma_{2n-3})}
$$

$$
\left. + \sum_{n=2}^{\infty} \frac{e^{-\gamma_{2n-3}(2L+D_1-D_5)} Y_{2n-3}^+ a_n p_n u_n^-}{b(\alpha + i\gamma_{2n-3})} \right], \qquad (71)
$$

where

$$
X_n^- = \frac{1}{G} \left\{ \left[e^{-2\Gamma_{1n}(D_2-D_1)} + \omega_{1n} \right] \left(\mu_1 + \frac{\mu_2 \Gamma_{3n}}{\Gamma_{2n}} \xi_{1n} \right) \right.
$$

$$
\cdot \left(\frac{k}{\mu_1} + S_4 \gamma_n \eta_{1n} \right) + \left[e^{-2\Gamma_{1n}(D_2-D_1)} + \omega_{1n} \right]
$$

$$
\left. \cdot \left(\mu_1 + \frac{\mu_2 \Gamma_{3n}}{\Gamma_{2n}} \xi_{1n}' \right) \left(\frac{k}{\mu_1} + S_4 \gamma_n \eta_{1n}' \right) \right\}, \qquad (72)
$$

$$
Y_n^- = \frac{1}{H} \left(\frac{\mu_1}{2\mu_2} + \frac{\Gamma_{1n}}{2\Gamma_{2n}} \tau_{1n}' \right) \left(\frac{R_4}{\mu_1} + \frac{\gamma_n S_4}{2} \chi_n \right)
$$

$$
\cdot \left[e^{-\Gamma_{1n}(D_2-D_1)} + e^{\Gamma_{1n}(D_2-D_1)} \tau_{1n}' \right], \qquad (73)
$$

$$
X_n^+ = \frac{32}{G} \frac{\mu_2 \mu_3}{\mu_4} \gamma_n \Gamma_{4n} e^{-\Gamma_{1n}(D_2-D_1)}
$$

$$
\cdot e^{-\Gamma_{2n}(D_3-D_2)} e^{-\Gamma_{4n}(D_5-D_4)} e^{-\Gamma_{3n}(D_4-D_3)}, \qquad (74)
$$

$$Y_n^+ = (1/H)[\mu_4\rho_{43n}(\gamma_n\rho_{4n} - 2)$$
$$+\Gamma_{4n}\rho_{4n} - \mu_4(\Gamma_{4n} + \gamma_n)e^{-2\Gamma_{4n}(D_5-D_4)}], \tag{75}$$

$$a_n = [(2n-3)\pi/2]^2/bi\gamma_{2n-3}, \quad p_n = b^{-1/2}M_+(i\gamma_{2n-3}), \tag{76}$$

$$u_n^- = b^{-1}U_-(-i\gamma_{2n-3}), \quad u_n^+ = b^{-1}U_{(+)}(i\gamma_{2n-3}), \tag{77}$$

$$J_u^{(1)}(\alpha) = \frac{1}{\pi i}\int_k^{k+i\infty} e^{2i\beta L}\frac{(\beta^2 - k^2)^{1/2}M_+(\beta)U_{(+)}(\beta)}{\beta - \alpha}d\beta, \tag{78}$$

$$J_u^{(2)}(\alpha) = \frac{1}{\pi i}\int_k^{k+i\infty} e^{2i\beta L}\frac{(\beta^2 - k^2)^{1/2}M_+(\beta)U_-(-\beta)}{\beta + \alpha}d\beta, \tag{79}$$

$$A_u = \frac{2b^{1/2}A\cos(kb\sin\theta_0)}{M_-(k\cos\theta_0)}, \quad B_u = \frac{2b^{1/2}B\cos(kb\sin\theta_0)}{M_+(k\cos\theta_0)}. \tag{80}$$

A similar decomposition procedure can also be applied to (54). Omitting the details, we arrive at

$$V_-(\alpha) = b^{1/2}N_-(\alpha)\left[-\frac{A_v}{b(\alpha - k\cos\theta_0)} + \frac{J_v^{(1)}(\alpha)}{b^{1/2}}\right.$$
$$-\sum_{n=2}^{\infty}\frac{e^{-2\gamma_{2n-2}(L+D_1)}X_{2n-2}^-b_nq_nv_n^-}{b(\alpha - i\gamma_{2n-2})}$$
$$\left.-\sum_{n=2}^{\infty}\frac{e^{-\gamma_{2n-2}(2L+D_1-D_5)}Y_{2n-2}^-b_nq_nv_n^+}{b(\alpha - i\gamma_{2n-2})}\right], \tag{81}$$

$$V_{(+)}(\alpha) = b^{1/2}N_+(\alpha)\left[\frac{B_v}{b(\alpha - k\cos\theta_0)} + \frac{J_v^{(2)}(\alpha)}{b^{1/2}}\right.$$
$$+\sum_{n=2}^{\infty}\frac{e^{-2\gamma_{2n-2}(L-D_5)}X_{2n-2}^+b_nq_nv_n^+}{b(\alpha + i\gamma_{2n-2})}$$
$$\left.+\sum_{n=2}^{\infty}\frac{e^{-\gamma_{2n-2}(2L+D_1-D_5)}Y_{2n-2}^+b_nq_nv_n^-}{b(\alpha + i\gamma_{2n-2})}\right], \tag{82}$$

where

$$b_n = [(n-1)\pi]^2/bi\gamma_{2n-2}, \quad q_n = b^{-1/2}N_+(i\gamma_{2n-2}), \tag{83}$$

$$v_n^- = b^{-1}V_-(-i\gamma_{2n-2}), \quad v_n^+ = b^{-1}V_{(+)}(i\gamma_{2n-2}), \tag{84}$$

$$J_v^{(1)}(\alpha) = \frac{1}{\pi i} \int_k^{k+i\infty} e^{2i\beta L} \frac{(\beta^2 - k^2)^{1/2} N_+(\beta) V_{(+)}(\beta)}{\beta - \alpha} d\beta, \quad (85)$$

$$J_v^{(2)}(\alpha) = \frac{1}{\pi i} \int_k^{k+i\infty} e^{2i\beta L} \frac{(\beta^2 - k^2)^{1/2} N_+(\beta) V_-(-\beta)}{\beta + \alpha} d\beta, \quad (86)$$

$$A_v = \frac{2ib^{1/2} A \sin(kb \sin \theta_0)}{N_-(k \cos \theta_0)}, \ B_v = \frac{2ib^{1/2} B \sin(kb \sin \theta_0)}{N_+(k \cos \theta_0)}. \quad (87)$$

Several coefficients appearing in (72)–(75) are defined in Appendix. Equations (70), (71) and (81), (82) are the exact solutions of the Wiener-Hopf equations (53) and (54), respectively, but they are formal since the infinite series with the unknown coefficients $u_n^\pm$ and $v_n^\pm$ for $n = 2, 3, 4, \ldots$ as well as the branch-cut integrals $J_u^{(1),(2)}(\alpha)$ and $J_v^{(1),(2)}(\alpha)$ with unknown integrands $U_-(\alpha)$, $U_{(+)}(\alpha)$, $V_-(\alpha)$, and $V_{(+)}(\alpha)$ are involved. Therefore, it is required to develop approximation procedures for an explicit solution.

5. APPROXIMATE SOLUTION

In this section, we shall evaluate the infinite series and branch-cut integrals occurring in the formal solutions to derive approximate solutions of the Wiener-Hopf equations. To this end, we can apply the method established in [19] for the analysis of the diffraction by a parallel-plate waveguide cavity.

First we shall derive an approximate expression of $U_-(\alpha)$ defined by (70). Assuming that the waveguide length $2L$ is large compared with the wavelength and applying the method in [19], the branch-cut integral $J_u^{(1)}(\alpha)$ defined by (78) can be expanded asymptotically as

$$J_u^{(1)}(\alpha) \sim J_u^{(11)}(\alpha) + J_u^{(12)}(\alpha) \quad (88)$$

for $kL \to \infty$, where

$$J_u^{(11)}(\alpha) = b^{1/2} a_1 p_1 \left[u_1^+ + \frac{2B \cos(kb \sin \theta_0)}{kb(1 - \cos \theta_0)} \right] \xi(-\alpha), \quad (89)$$

$$J_u^{(12)}(\alpha) = 2Lb^{-1/2} a_1 p_1 B \cos(kb \sin \theta_0) \frac{\xi(-\alpha) - \xi(-k \cos \theta_0)}{(-\alpha + k \cos \theta_0)L} \quad (90)$$

with

$$a_1 = kb, \quad p_1 = b^{-1/2} M_+(k), \quad u_1^+ = b^{-1} U_{(+)}(k), \quad (91)$$

$$\xi(\alpha) = \frac{e^{i(2kL - \pi/4)}}{\pi(kL)^{1/2}} \Gamma_1[3/2, -2i(\alpha + k)L]. \quad (92)$$

In (92) $\Gamma_1(\cdot, \cdot)$ is the generalized gamma function [27] defined by

$$\Gamma_m(u, v) = \int_0^\infty \frac{t^{u-1}e^{-t}}{(t+v)} dt \tag{93}$$

for $\mathrm{Re}\, u > 0, \quad |v| > 0, \quad |\arg v| < \pi$, and positive integer m.

Using (66), it is found that the coefficients $u_n^{\pm}$ defined by (77) show the asymptotic behavior

$$u_n^- \sim 2^{1/2}K_u^{(1)}(b\gamma_{2n-3})^{-3/2}, \quad u_n^+ \sim 2^{1/2}K_u^{(2)}(b\gamma_{2n-3})^{-3/2} \tag{94}$$

as $n \to \infty$, where $K_u^{(1)}$ and $K_u^{(2)}$ are unknown constants. Taking a large positive integer N and replacing $u_n^{\pm}$ for $n \geq N$ by their asymptotic behavior (94), each infinite series occurring in (70) can be approximated in reasonable accuracy by the sum of the finite series containing $N - 2$ unknowns and the infinite series with one unknown constant. This procedure yields an accurate approximate expression of the original infinite series since the edge condition is taken into account explicitly. Thus we arrive at the approximate expression of (70) with the result that

$$
\begin{aligned}
U_-(\alpha) \approx b^{1/2}M_-(\alpha) & \left(\frac{A_u}{b(\alpha - k\cos\theta_0)} \right. \\
& + a_1 p_1 \left\{ \left[u_1^+ + \frac{2B\cos(kb\sin\theta_0)}{kb(1-\cos\theta_0)} \right] \xi(-\alpha) \right. \\
& \left. + \frac{2LB}{b}\cos(kb\sin\theta_0)\frac{\xi(-\alpha) - \xi(-k\cos\theta_0)}{(-\alpha + k\cos\theta_0)L} \right\} \\
& - \sum_{n=2}^{N-1} \frac{a_n p_n X_{2n-3}^- e^{-2\gamma_{2n-3}(L+D_1)}u_n^-}{b(\alpha - i\gamma_{2n-3})} \\
& - \sum_{n=2}^{N-1} \frac{a_n p_n Y_{2n-3}^- e^{-\gamma_{2n-3}(2L+D_1-D_5)}u_n^+}{b(\alpha - i\gamma_{2n-3})} \\
& - K_u^{(1)} \sum_{n=N}^{\infty} \frac{a_n X_{2n-3}^-(b\gamma_{2n-3})^{-2}e^{-2\gamma_{2n-3}(L+D_1)}}{b(\alpha - i\gamma_{2n-3})} \\
& \left. - K_u^{(2)} \sum_{n=N}^{\infty} \frac{a_n Y_{2n-3}^-(b\gamma_{2n-3})^{-2}e^{-\gamma_{2n-3}(2L+D_1-D_5)}}{b(\alpha - i\gamma_{2n-3})} \right) \tag{95}
\end{aligned}
$$

for large N and $|k|\,L$.

A similar procedure can also be applied to derive approximate expressions of (71), (81), and (82). This leads to

$$U_{(+)}(\alpha) \approx b^{1/2} M_+(\alpha) \left(-\frac{B_u}{b\,(\alpha - k\cos\theta_0)} \right.$$

$$+ a_1 p_1 \left\{ \left[u_1^- + \frac{2A\cos(kb\sin\theta_0)}{kb\,(1 + \cos\theta_0)} \right] \xi(\alpha) \right.$$

$$+ \frac{2LA}{b}\cos(kb\sin\theta_0)\,\frac{\xi(\alpha) - \xi(k\cos\theta_0)}{(\alpha - k\cos\theta_0)L} \right\}$$

$$- \sum_{n=2}^{N-1} \frac{a_n p_n X_{2n-3}^+ e^{-2\gamma_{2n-3}(L-D_5)} u_n^+}{b\,(\alpha + i\gamma_{2n-3})}$$

$$+ \sum_{n=2}^{N-1} \frac{a_n p_n Y_{2n-3}^- e^{-\gamma_{2n-3}(2L+D_1-D_5)} u_n^-}{b\,(\alpha - i\gamma_{2n-3})}$$

$$+ K_u^{(2)} \sum_{n=N}^{\infty} \frac{a_n X_{2n-3}^+ (b\gamma_{2n-3})^{-2} e^{-2\gamma_{2n-3}(L-D_5)}}{b\,(\alpha + i\gamma_{2n-3})}$$

$$+ K_u^{(1)} \sum_{n=N}^{\infty} \frac{a_n Y_{2n-3}^+ (b\gamma_{2n-3})^{-2} e^{-\gamma_{2n-3}(2L+D_1-D_5)}}{b\,(\alpha + i\gamma_{2n-3})} \right), \quad (96)$$

$$V_-(\alpha) \approx b^{1/2} N_-(\alpha) \left(-\frac{A_v}{b\,(\alpha - k\cos\theta_0)} \right.$$

$$+ b_1 q_1 \left\{ \left[v_1^+ - \frac{2iB\sin(kb\sin\theta_0)}{kb\,(1 - \cos\theta_0)} \right] \xi(-\alpha) \right.$$

$$- \frac{2iLB}{b}\sin(kb\sin\theta_0)\,\frac{\xi(-\alpha) - \xi(-k\cos\theta_0)}{(-\alpha + k\cos\theta_0)L} \right\}$$

$$- \sum_{n=2}^{N-1} \frac{b_n q_n X_{2n-2}^- e^{-2\gamma_{2n-2}(L+D_1)} v_n^-}{b\,(\alpha - i\gamma_{2n-2})}$$

$$- \sum_{n=2}^{N-1} \frac{b_n q_n Y_{2n-2}^- e^{-\gamma_{2n-2}(2L+D_1-D_5)} v_n^+}{b\,(\alpha - i\gamma_{2n-2})}$$

$$- K_v^{(1)} \sum_{n=N}^{\infty} \frac{b_n X_{2n-2}^- (b\gamma_{2n-2})^{-2} e^{-2\gamma_{2n-2}(L+D_1)}}{b\,(\alpha - i\gamma_{2n-2})}$$

$$- K_v^{(2)} \sum_{n=N}^{\infty} \frac{b_n Y_{2n-2}^- (b\gamma_{2n-2})^{-2} e^{-\gamma_{2n-2}(2L+D_1-D_5)}}{b\,(\alpha - i\gamma_{2n-2})} \right), (97)$$

$$V_{(+)}(\alpha) \approx b^{1/2} N_+(\alpha) \left(\frac{B_v}{b\left(\alpha - k\cos\theta_0\right)} \right.$$

$$+ b_1 q_1 \left\{ \left[v_1^- + \frac{2iA\sin\left(kb\sin\theta_0\right)}{kb\left(1 + \cos\theta_0\right)} \right] \xi(\alpha) \right.$$

$$\left. - \frac{2iLA}{b}\sin\left(kb\sin\theta_0\right)\frac{\xi(\alpha) - \xi(k\cos\theta_0)}{(\alpha - k\cos\theta_0)L} \right\}$$

$$+ \sum_{n=2}^{N-1} \frac{b_n q_n X_{2n-2}^+ e^{-2\gamma_{2n-2}(L-D_5)} v_n^+}{b\left(\alpha + i\gamma_{2n-2}\right)}$$

$$+ \sum_{n=2}^{N-1} \frac{b_n q_n Y_{2n-2}^+ e^{-\gamma_{2n-2}(2L+D_1-D_5)} v_n^-}{b\left(\alpha + i\gamma_{2n-2}\right)}$$

$$+ K_v^{(2)} \sum_{n=N}^{\infty} \frac{b_n X_{2n-2}^- (b\gamma_{2n-2})^{-2} e^{-2\gamma_{2n-2}(L-D_5)}}{b\left(\alpha + i\gamma_{2n-2}\right)}$$

$$\left. + K_v^{(1)} \sum_{n=N}^{\infty} \frac{b_n Y_{2n-2}^+ (b\gamma_{2n-2})^{-2} e^{-\gamma_{2n-2}(2L+D_1-D_5)}}{b\left(\alpha + i\gamma_{2n-2}\right)} \right) \qquad (98)$$

for large N and $|k| L$, where

$$b_1 = kb, \quad q_1 = b^{-1/2} N_+(k), \qquad (99)$$

$$u_1^- = b^{-1} U_-(-k); \quad v_1^- = b^{-1} V_-(-k), \quad v_1^+ = b^{-1} V_{(+)}(k). \qquad (100)$$

In the derivation of (97) and (98), we have used the edge condition

$$v_n^- \sim 2^{1/2} K_v^{(1)} \left(b\gamma_{2n-2}\right)^{-3/2}, \quad u_n^+ \sim 2^{1/2} K_v^{(2)} \left(b\gamma_{2n-2}\right)^{-3/2} \qquad (101)$$

for $n \to \infty$, where $K_v^{(1)}$ and $K_v^{(2)}$ are unknown constants.

Equations (95), (96) and (97), (98) are approximate solutions to the Wiener-Hopf Equations (53) and (54), respectively, and they are valid for large positive integer N and large $|k| L$. The unknown $u_n^{\pm}$ and $v_n^{\pm}$ for $n = 1, 2, \ldots, N-1$ and $K_u^{(1),(2)}$, $K_v^{(1),(2)}$ in (95)–(98) are determined with high accuracy by solving appropriate $2N \times 2N$ matrix equations numerically.

6. SCATTERED FIELD

The scattered field can be derived by taking the inverse Fourier transform of (48) according to the formula

$$\phi(x, z) = (2\pi)^{-1/2} \int_{-\infty+ic}^{\infty+ic} \Phi(x, \alpha) e^{-i\alpha z} d\alpha, \qquad (102)$$

where $|c| < k_2 \cos \theta_0$. First let us consider the field inside the waveguide. Substituting the field representation for $|x| < b$ in (48) into (102) and evaluating the resultant integral, we find from (1) that the total field for the region inside the waveguide is expressed in terms of the TE modes and takes the form

$$\phi^t(x,\,z) = \sum_{n=1}^{\infty} \left[T_{Ln}^+ e^{\gamma_n(z-D_1)} - T_{Ln}^- e^{-\gamma_n(z-D_1)} \right] \sin \frac{n\pi}{2b}(x+b)$$

$$\text{for} -L < z < D_1,$$

$$= \sum_{n=1}^{\infty} \left[T_{mn}^+ e^{\Gamma_m(z-D_m)} - T_{mn}^- e^{-\Gamma_m(z-D_m)} \right] \sin \frac{n\pi}{2b}(x+b)$$

$$\text{for} \, D_m < z < D_{m+1},\, m = 1,\, 2,\, 3,\, 4,$$

$$= \sum_{n=1}^{\infty} \left[T_{Rn}^+ e^{\gamma_n(z-D_5)} - T_{Rn}^- e^{-\gamma_n(z-D_5)} \right] \sin \frac{n\pi}{2b}(x+b)$$

$$\text{for} \, D_5 < z < L, \tag{103}$$

where

$$T_{Ln}^- = -\chi_n e^{-\gamma_n(L+D_1)} U_-(-i\gamma_n) \quad \text{for odd } n,$$

$$= \chi_n e^{-\gamma_n(L+D_1)} V_-(-i\gamma_n) \quad \text{for even } n, \tag{104}$$

$$T_{Ln}^+ = -\chi_n \left[X_n^- e^{-\gamma_n(L+D_1)} U_-(-i\gamma_n) + Y_n^- e^{-\gamma_n(L-D_5)} U_{(+)}(i\gamma_n) \right]$$

$$\text{for odd } n,$$

$$= \chi_n \left[X_n^- e^{-\gamma_n(L+D_1)} V_-(-i\gamma_n) + Y_n^- e^{-\gamma_n(L-D_5)} V_{(+)}(i\gamma_n) \right]$$

$$\text{for even } n, \tag{105}$$

$$T_{Rn}^- = \chi_n \left[Y_n^+ e^{-\gamma_n(L+D_1)} U_-(-i\gamma_n) + X_n^- e^{-\gamma_n(L-D_5)} U_{(+)}(i\gamma_n) \right]$$

$$\text{for odd } n,$$

$$= -\chi_n \left[Y_n^+ e^{-\gamma_n(L+D_1)} V_-(-i\gamma_n) + X_n^- e^{-\gamma_n(L-D_5)} V_{(+)}(i\gamma_n) \right]$$

$$\text{for even } n, \tag{106}$$

$$T_{Rn}^+ = \chi_n e^{-\gamma_n(L-D_5)} U_{(+)}(i\gamma_n) \quad \text{for odd } n,$$

$$= -\chi_n e^{-\gamma_n(L-D_5)} V_{(+)}(i\gamma_n) \quad \text{for even } n, \tag{107}$$

$$T_{mn}^- = -K_{mn} \left[R_{mn}^- U_-(-i\gamma_n) + S_{mn}^- U_{(+)}(i\gamma_n) \right]$$

$$\text{for odd } n \, (m = 1,\, 2,\, 3,\, 4),$$

$$= K_{mn} \left[R_{mn}^- V_-(-i\gamma_n) + S_{mn}^- V_{(+)}(i\gamma_n) \right]$$

$$\text{for even } n \, (m = 1,\, 2,\, 3,\, 4), \tag{108}$$

$$T_{mn}^+ = -K_{mn}\left[R_{mn}^+ U_-(-i\gamma_n) + S_{mn}^+ U_{(+)}(i\gamma_n)\right]$$
$$\text{for odd } n \ (m = 1, 2, 3, 4),$$
$$= K_{mn}\left[R_{mn}^+ V_-(-i\gamma_n) + S_{mn}^+ V_{(+)}(i\gamma_n)\right]$$
$$\text{for even } n \ (m = 1, 2, 3, 4), \tag{109}$$

$$R_{1n}^- = P_{1n} - \Gamma_{1n}R_{1n}, \ R_{1n}^+ = (\mu_1/\mu_2)P_{2n} + \Gamma_{1n}R_{2n},$$
$$S_{1n}^- = Q_{1n} - \Gamma_{1n}S_{1n}, \ S_{1n}^+ = (\mu_1/\mu_2)Q_{2n} + \Gamma_{1n}S_{2n}, \tag{110}$$
$$R_{2n}^- = P_{2n} - \Gamma_{2n}R_{2n}, \ R_{2n}^+ = P_{3n} + \Gamma_{2n}R_{3n}, \tag{111}$$
$$S_{2n}^- = Q_{2n} - \Gamma_{2n}S_{2n}, \ S_{2n}^+ = Q_{3n} + \Gamma_{2n}S_{3n}, \tag{112}$$
$$R_{3n}^- = (\mu_3/\mu_2)P_{3n} - \Gamma_{3n}R_{3n}, \ R_{3n}^+ = P_{4n} + \Gamma_{3n}R_{4n}, \tag{113}$$
$$S_{3n}^- = (\mu_3/\mu_2)Q_{3n} - \Gamma_{3n}S_{3n}, \ S_{3n}^+ = Q_{4n} + \Gamma_{3n}S_{4n}, \tag{114}$$
$$R_{4n}^- = (\mu_4/\mu_3)P_{4n} - \Gamma_{4n}R_{4n}, \ R_{4n}^- = (\mu_4/\mu_3)P_{4n} + \Gamma_{4n}R_{4n}, \tag{115}$$
$$S_{4n}^- = (\mu_4/\mu_3)Q_{4n} - \Gamma_{4n}S_{4n}, \ S_{4n}^+ = (\mu_4/\mu_3)Q_{4n} + \Gamma_{4n}R_{4n}, \tag{116}$$
$$\chi_n = \left(\frac{\pi}{2}\right)^{1/2}\frac{n\pi}{2b^2\gamma_n}; \ K_{mn} = \left(\frac{\pi}{2}\right)^{1/2}\frac{n\pi}{2b^2\Gamma_{mn}} \text{ for } m = 1, 2, 3, 4, \tag{117}$$

In (110)–(114), the definition of P_{mn}, Q_{mn}, R_{mn}, and S_{mn} for $m = 1, 2, 3, 4$ is given in Appendix.

Next we shall consider the field outside the waveguide and derive the scattered far field. Substituting the field representation for $|x| > b$ in (48) into (102) and evaluating the resultant integral asymptotically with the aid of the saddle point method, we obtain a far field expression

$$\phi(\rho, \theta) \sim \Psi(\pm b, -k\cos\theta)k\sin\theta e^{\pm ikb\sin\theta}\frac{e^{i(k\rho-\pi/4)}}{(k\rho)^{1/2}} \tag{118}$$

for $x \gtrless \pm b$ as $k\rho \to \infty$, where (ρ, θ) is the cylindrical coordinate defined by $x = \rho\sin\theta$, $z = \rho\cos\theta$ for $0 < |\theta| < \pi$. In (119), $\Psi(\pm b, \alpha)$ is expressed as

$$\Psi(\pm b, \alpha) = e^{-i\alpha L}\frac{U_-(\alpha) \pm V_-(\alpha)}{2} + e^{i\alpha L}\frac{U_{(+)}(\alpha) \pm V_{(+)}(\alpha)}{2} \tag{119}$$

by making use of (11) and (55)–(58). Although (119) has been derived only for the region $|x| > b$ (i.e., $0 < |\theta| < \pi$), it can be shown that (119) is continuous across $|\theta| = 0, \pi$. Therefore, (119) is valid for arbitrary θ. The analysis has thus far been carried out by assuming that $0 < \theta_0 < \pi/2$, but the result is in fact true for arbitrary θ_0.

7. NUMERICAL RESULTS AND DISCUSSION

In this section, we shall show representative numerical examples of the RCS for various physical parameters to discuss the far field scattering characteristics of the waveguide in detail. Numerical results presented below are based on the use of the scattered far field expression as given by (119) together with (120). We have used the approximate expressions as derived in (95)–(98) for computing the functions $U_-(\alpha)$, $U_{(+)}(\alpha)$, $V_-(\alpha)$, and $V_{(+)}(\alpha)$ involved in (120). As has been mentioned at the end of Section 5, we need to solve the two sets of $2N \times 2N$ matrix equations numerically for obtaining all the physical quantities. According to the theory of the Wiener-Hopf technique, convergence of the approximate solutions obtained in Section 5 is very fast for a small waveguide aperture $2b$, since we then do not require large N in numerical computation. In order for the approximate solutions to be reasonably accurate, however, some large N is needed with an increase of $2b$. By careful numerical experimentation, we have verified that sufficiently accurate results can be obtained by choosing $N \geq 2kb/\pi$ in (95)–(98).

We shall now investigate the scattering mechanism via numerical results of the monostatic and bistatic RCS for various physical parameters. Since the problem considered here is of the two-dimensional scattering, the RCS per unit length is defined by

$$\sigma = \lim_{\rho \to \infty} \left(2\pi\rho \, |\phi|^2 / \left|\phi^i\right|^2 \right). \tag{120}$$

For real k, (121) is simplified by using (2) and (118) as

$$\sigma = \lambda \left| \Psi(\pm b, -k\cos\theta)k\sin\theta \right|^2, \quad \theta \gtrless 0, \tag{121}$$

where λ is the free-space wavelength.

Figures 3 and 4 show the monostatic RCS σ/λ as a function of incident angle θ_0 where the values of σ/λ are plotted in decibels [dB] by computing $10\log_{10}\sigma/\lambda$. The waveguide structure is symmetric along the z-axis so that we have presented the RCS data only for the range $0° \leq \theta_0 \leq 180°$. In order to investigate the scattering mechanism over a broad frequency range, we have carried out numerical computation for three typical values of the normalized waveguide aperture width $kb = 3.14, 15.7$, and 31.4, which correspond to low, medium, and high frequencies, respectively. For a fixed kb, the ratio of the waveguide length $2L$ to the waveguide aperture width $2b$ has been chosen as $L/b = 1.0, 3.0$. In numerical computation, we have considered the case where layer I $(D_1 < z < D_2)$ is filled with perfect conductors so that two cavity regions are formed at the left $(-L < z < D_1)$
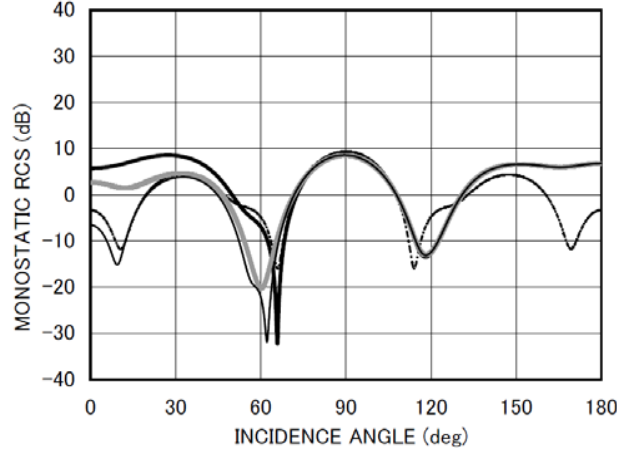
Figure 3a. Monostatic RCS σ/λ [dB] for $L/b = 1.0$, $kb = 3.14$.
-·-·-·-·-·- empty waveguide (layers I-IV: vacuum). ————: cavity
with no loading (layer I: perfect conductor; layers II-IV: vacuum;
$t_L = 0.6\,L$, $t_{\text{PEC}} = 0.4L$, $t_R = L$). ————: cavity with two-layer
loading (layer I: perfect conductor; layer II: $\varepsilon_2 = 3.14+i10.0$, $\mu_2 = 1.0$;
layer III: $\varepsilon_3 = 1.6+i0.9$, $\mu_3 = 1.0$; layer IV: vacuum; $t_L = 0.6L$, $t_{\text{PEC}} =$
$0.4L$, $t_R = L$, $t_{2\text{layer}} = 0.4L$). ————: cavity with three-layer loading
(layer I: perfect conductor; layers II-IV: Emerson & Cuming AN-73;
$t_L = 0.6L$, $t_{\text{PEC}} = 0.4L$, $t_R = L$, $t_{3\text{layer}} = 0.6L$).

Figure 3b. Monostatic RCS σ/λ [dB] for $L/b = 1.0$, $kb = 15.7$. Other
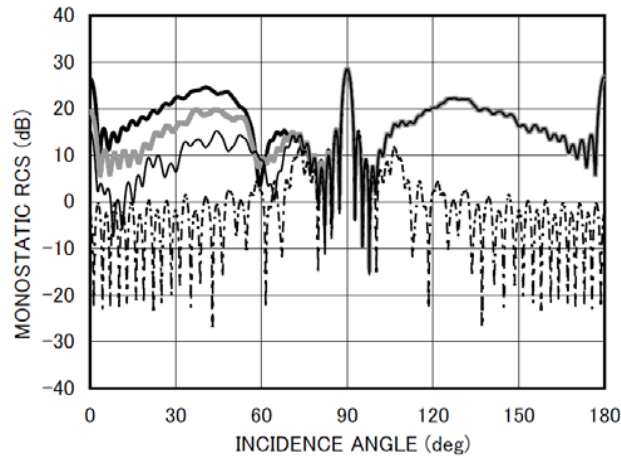particulars are the same as in Fig. 3a.

Figure 3c. Monostatic RCS σ/λ [dB] for $L/b = 1.0$, $kb = 31.4$. Other particulars are the same as in Fig. 3a.
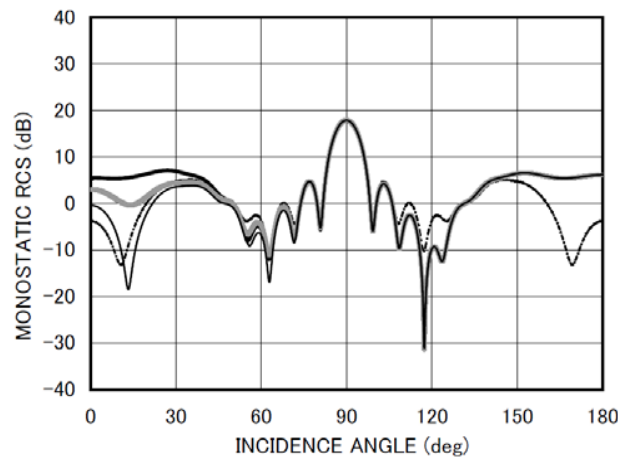

Figure 4a. Monostatic RCS σ/λ [dB] for $L/b = 3.0$, $kb = 3.14$. Other particulars are the same as in Fig. 3a.

and right $(D_2 < z < L)$ sides of the waveguide. We have chosen the depth of the left and right cavities as $t_L(= D_1 + L) = 0.6L$ and $t_R(= L - D_2) = L$, respectively so that the thickness of layer I (perfect conductors) becomes $t_{PEC}(= D_2 - D_1) = 0.4L$. In order to investigate the effect of the three-layer material loading, we have considered the case where layers II–IV in the right cavity are composed of Emerson &
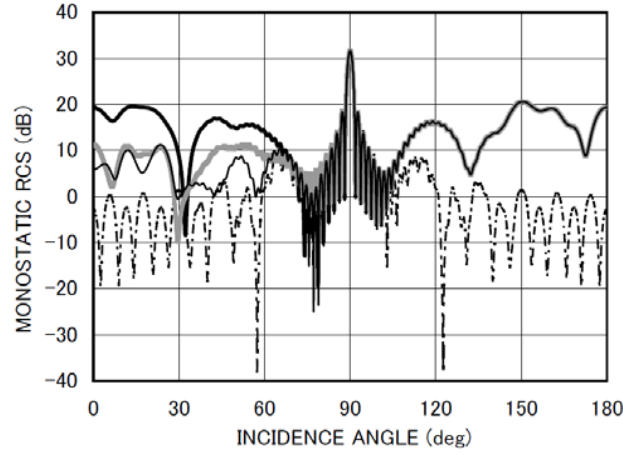
Figure 4b. Monostatic RCS σ/λ [dB] for $L/b = 3.0$, $kb = 15.7$. Other particulars are the same as in Fig. 3a.
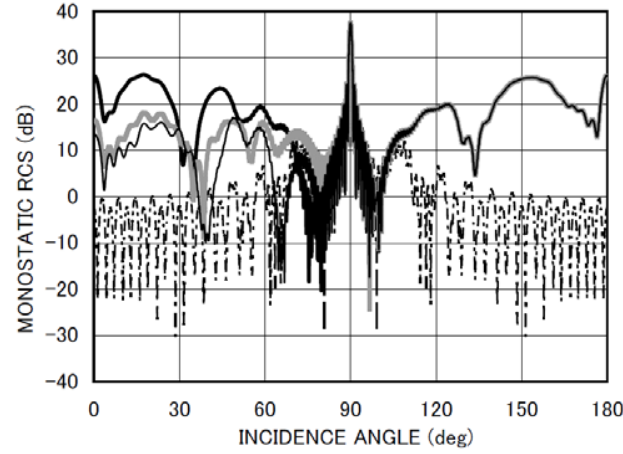

Figure 4c. Monostatic RCS σ/λ [dB] for $L/b = 3.0$, $kb = 31.4$. Other particulars are the same as in Fig. 3a.

Cuming AN-73 [2] with the material constants being $\varepsilon_2 = 3.14 + i10.0$, $\mu_2 = 1.0$, $\varepsilon_3 = 1.6 + i0.9$, $\mu_3 = 1.0$, $\varepsilon_4 = 1.4 + i0.35$, $\mu_4 = 1.0$ and the layer thickness being $D_3 - D_2 = D_4 - D_3 = D_5 - D_4$ $(= t_{3\text{layer}}/3)$. We have also considered the two-layer case where layer IV of Emerson & Cuming AN-73 is removed, namely, $\varepsilon_2 = 3.14 + i10.0$, $\mu_2 = 1.0$, $\varepsilon_3 = 1.6 + i0.9$, $\mu_3 = 1.0$, $\varepsilon_4 = \mu_4 = 1.0$, and $D_3 - D_2 = D_4 - D_3$ $(= t_{2\text{layer}}/2)$. The thickness of the two- and three-layer materials has been taken as

$t_{2\text{layer}} = 0.4L$ and $t_{3\text{layer}} = 0.6L$, respectively. In addition, the results for an empty parallel-plate waveguide ($\varepsilon_n = \mu_n = 1.0$, $n = 1, 2, 3, 4$) have also been plotted for comparison.

It is seen from Figs. 3 and 4 that the monostatic RCS exhibits sharp peaks at $\theta_0 = 90°$, which correspond to the specular reflection from the upper waveguide plate at $x = b$. Due to the geometrical symmetry, the RCS curves for the parallel-plate waveguide with no material loading are symmetrical around the main lobe direction at $\theta_0 = 90°$. For fairly large square-shape cavities ($L/b = 1.0$) with no material loading, the RCS takes close values at $\theta_0 = 0°$, $90°$, $180°$ as seen from Figs. 3(b) and 3(c), since contributions to the backscattered far field at high frequencies mainly come from the reflected waves from the perfectly conducting surfaces at $x = b$ and $z = D_1$, D_2.

We find from the four curves in Figs. 3 and 4 that the RCS characteristics of all the waveguide geometries for fixed kb and L/b show close features near the main lobe direction $80° < \theta_0 < 100°$. This is because main contributions to the backscattered far field arise from exterior features of the waveguide, not depending on features inside the waveguide. We also notice from the results of the three cavities for fixed kb and L/b that the RCS characteristics for $90° < \theta_0 < 180°$ are nearly identical to each other, since the cavity formed at the right side of the waveguide is then invisible from the incident direction and the backscattered far field is not affected by the interior geometries of the right cavity.

We now investigate the effect of material loading inside the right cavity. For the cavity with no material loading, the RCS shows large values over the range $0° < \theta_0 < 80°$ due to the interior irradiation, whereas the irradiation is reduced for the case of material loading. By comparing the RCS results for material-loaded cavities between the two-layer case and the three-layer case (Emerson & Coming AN-73), we see better RCS reduction in the case of the cavity with three-layer loading for all chosen kb and L/b. Incidentally, the empty parallel-plate waveguide for large kb ($= 15.7$, 31.4) shows very low RCS values except in the neighborhood of $\theta_0 = 90°$ because only the edge-diffracted fields contribute to the backscattered far field.

Figures 5 and 6 show the bistatic RCS σ/λ [dB] as a function of observation angle θ, where the incidence angle is chosen as $\theta_0 = 45°$, and other parameters are the same as in Figs. 3 and 4. From Figs. 5 and 6, it is found that the bistatic RCS shows noticeable peaks at $\theta = -135°$ and $\theta = 135°$ for all the four waveguide geometries, which correspond to the incident and reflected shadow boundaries, respectively. It is also seen that, for $L/b = 1.0$ and $kb = 15.7$, 31.4, the peak RCS values at $\theta = 135°$ for the empty parallel-plate waveguide are somewhat larger

than those for the other three geometries (cavities with and without material loading) as seen from Figs. 5(b) and 5(c). This is because contributions to the scattered far field along the $\theta = 135°$ direction for the empty parallel-plate waveguide arise due to the specular reflection
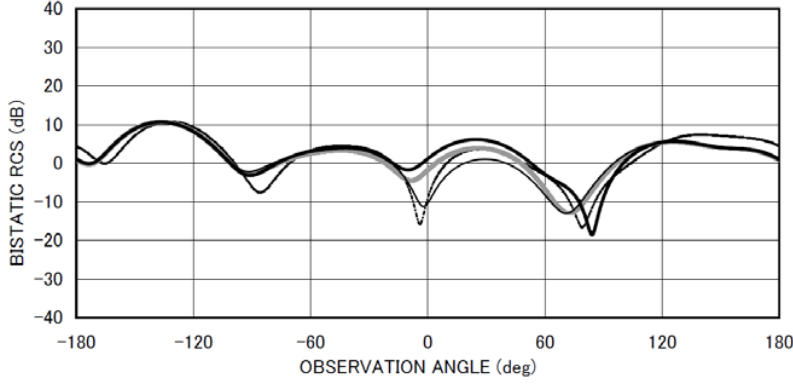

Figure 5a. Bistatic RCS σ/λ [dB] for $L/b = 1.0$, $kb = 3.14$, $\theta_0 = 45°$. ·--·--·--·-- empty waveguide (layers I-IV: vacuum). ———: cavity with no loading (layer I: perfect conductor; layers II-IV: vacuum; $t_L = 0.6\,L$, $t_{\mathrm{PEC}} = 0.4L$, $t_R = L$). ———: cavity with two-layer loading (layer I: perfect conductor; layer II: $\varepsilon_2 = 3.14+i10.0$, $\mu_2 = 1.0$; layer III: $\varepsilon_3 = 1.6+i0.9$, $\mu_3 = 1.0$; layer IV: vacuum; $t_L = 0.6L$, $t_{\mathrm{PEC}} = 0.4L$, $t_R = L$, $t_{2\mathrm{layer}} = 0.4L$). ———: cavity with three-layer loading (layer I: perfect conductor; layers II-IV: Emerson & Cuming AN-73; $t_L = 0.6L$, $t_{\mathrm{PEC}} = 0.4L$, $t_R = L$, $t_{3\mathrm{layer}} = 0.6L$).
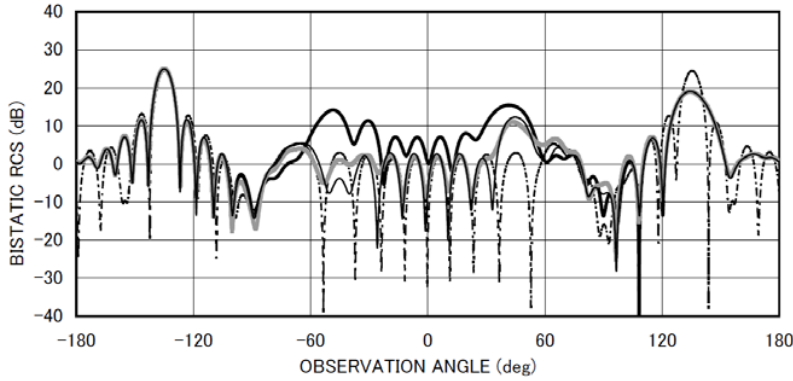

Figure 5b. Bistatic RCS σ/λ [dB] for $L/b = 1.0$, $kb = 15.7$, $\theta_0 = 45°$. Other particulars are the same as in Fig. 5a.
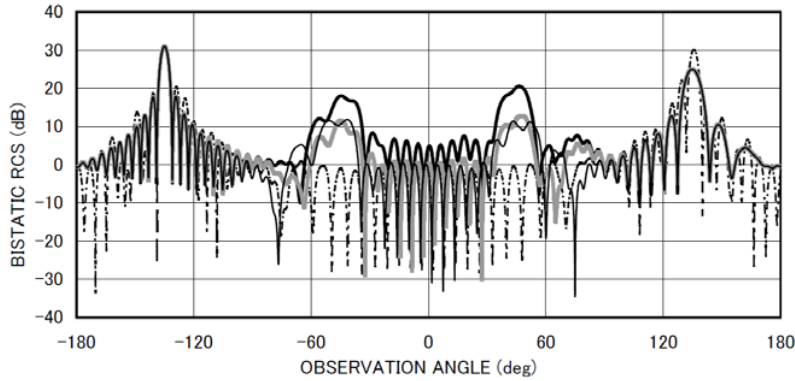
Figure 5c. Bistatic RCS σ/λ [dB] for $L/b = 1.0$, $kb = 31.4$, $\theta_0 = 45°$. Other particulars are the same as in Fig. 5a.
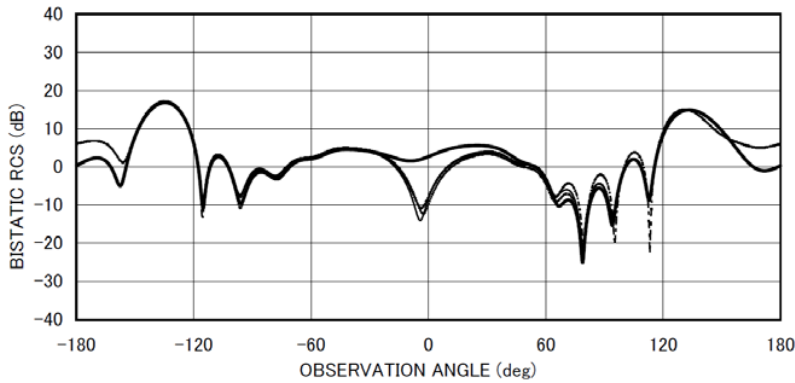

Figure 6a. Bistatic RCS σ/λ [dB] for $L/b = 3.0$, $kb = 3.14$, $\theta_0 = 45°$. Other particulars are the same as in Fig. 5a.

from both the upper and lower plates, but the reflected waves from the lower plate do not contribute to the bistatic scattering in the case of cavities. By comparing Figs. 5 and 6, we find that the peaks at $\theta = \pm 135°$ become sharper with an increase of L/b as expected. It is also observed that, when $L/b = 3.0$, the RCS of the parallel-plate waveguide and the cavities at $\theta = 135°$ shows close values as the reflected waves from the lower plate then do not contribute much to the scattered far field unlike the case of $L/b = 1.0$. The other feature in Figs. 5 and 6 is that there are some peaks in the neighborhood of $\theta = \pm 45°$ for larger cavities with no material loading, which are caused by the reradiation of the waveguide modal fields.
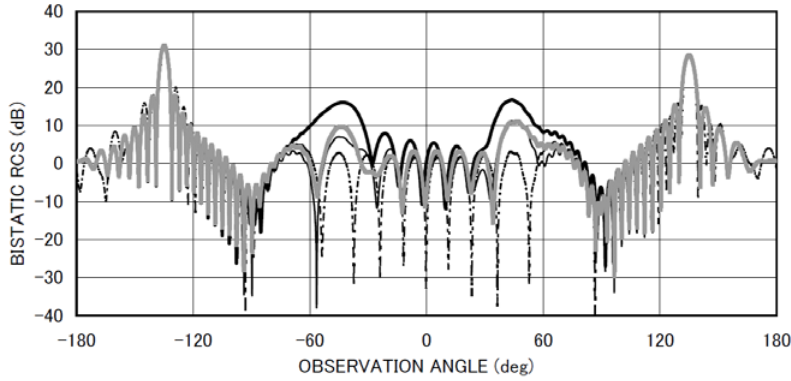
Figure 6b. Bistatic RCS σ/λ [dB] for $L/b = 3.0$, $kb = 15.7$, $\theta_0 = 45°$. Other particulars are the same as in Fig. 5a.
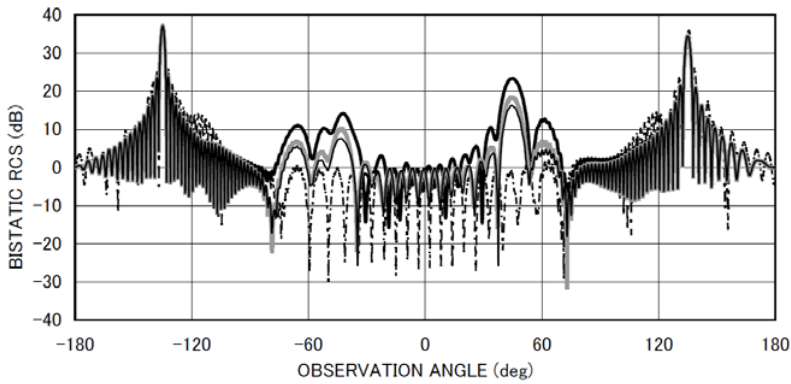

Figure 6c. Bistatic RCS σ/λ [dB] for $L/b = 3.0$, $kb = 31.4$, $\theta_0 = 45°$. Other particulars are the same as in Fig. 5a.

On comparing the results for the empty cavity with those for the material-loaded cavities, we notice that the RCS of cavities with and without material loading show close features over $|\theta| > 90°$, since the scattered far field is not affected by the interior geometries of the right cavity. On the other hand, there are significant differences in the range $|\theta| < 90°$, where a noticeable RCS reduction occurs for the material-loaded cavities. According to the results presented in Figs. 5 and 6, we also see that, for large kb, the bistatic RCS of the cavity with three-layer loading shows more significant RCS reduction than the two-layer case in $|\theta| < 60°$.

8. CONCLUSIONS

In this paper, we have considered a finite parallel-plate waveguide with four-layer loading as a generalization to the geometry treated in our previous papers [24, 25], and analyzed rigorously the E-polarized plane wave diffraction by means of the Wiener-Hopf technique. We have obtained exact and approximate solutions to the Wiener-Hopf equations. Since the approximate solution has been derived on the basis of a rigorous asymptotics, our final results are valid for the waveguide length large compared with the incident wavelength. We have presented illustrative numerical examples of the monostatic and bistatic RCS for various physical parameters to discuss the far field scattering characteristics in detail. In particular, it has been shown that the four-layer material loading gives rise to a better RCS reduction compared with the three-layer case analyzed in our previous papers. The results can be used as a reference solution for validating more general but approximate approaches. A similar Wiener-Hopf analysis for the case of the H-polarized plane wave incidence is carried out in the companion paper [26].

ACKNOWLEDGMENT

APPENDIX A. ANALYTICAL PROPERTIES OF THE FOURIER COEFFICIENTS

This appendix concerns the derivation of important formulas for the Fourier coefficients, which play an essential role in solving the Wiener-Hopf equations. We first note that $\Psi_-(x, \alpha)$ is regular in $\tau < k_2 \cos\theta_0$ (see (8) and (13)) and $\Psi_{(+)}(x, \alpha)$ is regular in $\tau > -k_2 \cos\theta_0$ except for a simple pole at $\alpha = k\cos\theta_0$ (see (8) and (14)), whereas $\Phi_m(x, \alpha)$ for $m = 1, 2, 3, \ldots, 6$ are entire functions (see (9)). Hence, we deduce that

$$\lim_{\alpha \to -i\gamma_n} (\alpha + i\gamma_n) \left[\Phi_1(x, \alpha) + e^{-i\alpha L}\Psi_-(x, \alpha) \right] = 0, \qquad \text{(A1)}$$

$$\lim_{\alpha \to i\gamma_n} (\alpha - i\gamma_n) \left[\Phi_6(x, \alpha) + e^{i\alpha L}\Psi_{(+)}(x, \alpha) \right] = 0, \qquad \text{(A2)}$$

$$\lim_{\alpha \to \pm i\Gamma_{mn}} (\alpha \mp i\Gamma_{m-1, n})\Phi_m(x, \alpha) = 0, \ m = 2, 3, 4, 5 \qquad \text{(A3)}$$

for $n = 1, 2, 3, \ldots$ Substituting (38), (39), and (40) into (A1), (A2), and (A3), respectively, we derive, after some manipulations, that

$$c_{1n}^{-}(-i\gamma_n) = -\frac{n\pi}{2b}e^{-\gamma_n(L+D_1)}U_-(-i\gamma_n) \text{ for odd } n,$$

$$= \frac{n\pi}{2b}e^{-\gamma_n(L+D_1)}V_-(-i\gamma_n) \text{ for even } n, \quad (A4)$$

$$c_{5n}^{+}(i\gamma_n) = \frac{n\pi}{2b}e^{-\gamma_n(L-D_5)}U_{(+)}(i\gamma_n) \text{ for odd } n,$$

$$= -\frac{n\pi}{2b}e^{-\gamma_n(L-D_5)}V_{(+)}(i\gamma_n) \text{ for even } n, \quad (A5)$$

$$c_{mn}^{+}(i\Gamma_{mn}) - e^{-\Gamma_{mn}(D_{m+1}-D_m)}c_{m+1,\,n}^{-}(i\Gamma_{mn}) = 0$$
$$\text{for} \quad n = 1, 2, 3, \ldots, \quad (A6)$$

$$e^{-\Gamma_{mn}(D_{m+1}-D_m)}c_{mn}^{+}(-i\Gamma_{mn}) - c_{m+1,\,n}^{-}(-i\Gamma_{mn}) = 0$$
$$\text{for} \quad n = 1, 2, 3, \ldots. \quad (A7)$$

Equations (A4)–(A7) constitute a system of simultaneous algebraic equations, which relates the Fourier coefficients f_{mn} and g_{mn} for $m = 1, 2, 3, 4, 5$ with the functions $U_-(\alpha)$, $U_{(+)}(\alpha)$, $V_-(\alpha)$, and $V_{(+)}(\alpha)$. Solving these equations for f_{mn} and g_{mn} for $m = 1, 2, 3, 4, 5$, we are led to

$$f_{mn} = -\frac{n\pi}{2b}\left[e^{-\gamma_n(L+D_1)}P_{mn}U_-(-i\gamma_n)+e^{-\gamma_n(L-D_5)}Q_{mn}U_{(+)}(i\gamma_n)\right]$$
$$\text{for odd } n,$$

$$= \frac{n\pi}{2b}\left[e^{-\gamma_n(L+D_1)}P_{mn}V_-(-i\gamma_n) + e^{-\gamma_n(L-D_5)}Q_{mn}V_{(+)}(i\gamma_n)\right]$$
$$\text{for even } n, \quad (A8)$$

$$g_{mn} = -\frac{n\pi}{2b}\left[e^{-\gamma_n(L+D_1)}R_{mn}U_-(-i\gamma_n) + e^{-\gamma_n(L-D_5)}S_{mn}U_{(+)}(i\gamma_n)\right]$$
$$\text{for odd } n,$$

$$= \frac{n\pi}{2b}\left[e^{-\gamma_n(L+D_1)}R_{mn}V_-(-i\gamma_n) + e^{-\gamma_n(L-D_5)}S_{mn}V_{(+)}(i\gamma_n)\right]$$
$$\text{for even } n, \quad (A9)$$

where

$$P_{5n} = (16/G)\mu_2\mu_3\gamma_n\Gamma_{4n}e^{-\Gamma_{4n}(D_5-D_4)}e^{-\Gamma_{3n}(D_4-D_3)}$$
$$\cdot e^{-\Gamma_{2n}(D_3-D_2)}e^{-\Gamma_{1n}(D_2-D_1)}, \quad (A10)$$

$$Q_{5n} = (1/H)\left\{\gamma_n\mu_4^2\rho_{43n}(\rho_{4n}-1)\right.$$
$$\left.+\mu_4\gamma_n\left[\rho_{43n}\rho_{4n} - e^{-2\Gamma_{4n}(D_5-D_4)}\right]\right\}, \quad (A11)$$

$$R_{5n} = (16/G)(\mu_2\mu_3/\mu_4)\gamma_n\Gamma_{4n}e^{-\Gamma_{4n}(D_5-D_4)}$$
$$\cdot e^{-\Gamma_{3n}(D_4-D_3)}e^{-\Gamma_{2n}(D_3-D_2)}e^{-\Gamma_{1n}(D_2-D_1)}, \quad (A12)$$

$$S_{5n} = -(1/H)\mu_4[\rho_{43n} - e^{-2\Gamma_{4n}(D_5-D_4)}], \quad (A13)$$

$$P_{4n} = (8/G)\mu_2\Gamma_{4n}(\mu_4\gamma_n + \Gamma_{4n})e^{-\Gamma_{3n}(D_4-D_3)}$$
$$\cdot e^{-\Gamma_{2n}(D_3-D_2)}e^{-\Gamma_{1n}(D_2-D_1)}\left[e^{-2\Gamma_{4n}(D_5-D_4)} + \rho_{4n}\right], \quad (A14)$$

$$Q_{4n} = -\frac{1}{H}\left[\frac{\mu_4}{\mu_3}\Gamma_{4n}(\rho_{43n} + \mu_4)e^{-\Gamma_{4n}(D_5-D_4)}\right.$$
$$\left.-\mu_4\rho_{43n}(\rho_{4n} + 1)\left(\gamma_n\frac{\mu_4^2}{2\mu_3}\delta_{4n} + \Gamma_{4n}\right)e^{\Gamma_{4n}(D_5-D_4)}\right], \quad (A15)$$

$$R_{4n} = (8/G)(\mu_2\mu_3/\mu_4)(\mu_4\gamma_n + \Gamma_{4n})e^{-\Gamma_{3n}(D_4-D_3)}$$
$$\cdot e^{-\Gamma_{2n}(D_3-D_2)}e^{-\Gamma_{1n}(D_2-D_1)}[e^{-2\Gamma_{4n}(D_5-D_4)} - \rho_{4n}], \quad (A16)$$

$$S_{4n} = \frac{1}{H}\left[\mu_4(\rho_{43n} - 1)e^{-\Gamma_{4n}(D_5-D_4)} - \frac{\mu_4}{2}\rho_{43n}\right.$$
$$\left.\cdot(\rho_{4n} + 1)\left(\frac{\gamma_n}{\Gamma_{4n}}\mu_4\delta_{4n} + 1\right)e^{\Gamma_{4n}(D_5-D_4)}\right], \quad (A17)$$

$$P_{3n} = \frac{1}{G}\frac{4\mu_2^2}{\mu_3\mu_4}(\mu_4\gamma_n + \Gamma_{4n})\left(\frac{\mu_3\Gamma_{3n}}{\mu_4} + \Gamma_{4n}\right)e^{-\Gamma_{2n}(D_3-D_2)}$$
$$\cdot e^{-\Gamma_{1n}(D_2-D_1)}\left\{e^{-2\Gamma_{4n}(D_5-D_4)}\left[e^{-2\Gamma_{3n}(D_4-D_3)} + \rho_{3n}\right]\right.$$
$$\left.+\rho_{3n}\rho_{4n}\left[e^{-2\Gamma_{3n}(D_4-D_3)} + 1\right]\right\}, \quad (A18)$$

$$Q_{3n} = \frac{1}{H}\left\{\frac{\mu_2 I}{2\mu_3}e^{-\Gamma_{4n}(D_5-D_4)}\left[x_{3n}e^{-\Gamma_{3n}(D_4-D_3)} - e^{\Gamma_{3n}(D_4-D_3)}\right]\right.$$
$$+\frac{\mu_2 J}{2\mu_3}\rho_{4n+1}e^{\Gamma_{4n}(D_5-D_4)}$$
$$\left.\left[y_{3n}e^{-\Gamma_{3n}(D_4-D_3)} + e^{\Gamma_{3n}(D_4-D_3)}\right]\right\}, \quad (A19)$$

$$R_{3n} = (1/G)((4\mu_2/\Gamma_{3n})(\mu_4\gamma_n+\Gamma_{4n})\left[(\mu_3\Gamma_{3n}/\mu_4)+\Gamma_{4n}\right]$$
$$\cdot e^{-\Gamma_{2n}(D_3-D_2)}e^{-\Gamma_{1n}(D_2-D_1)}\left\{e^{-2\Gamma_{4n}(D_5-D_4)}\right.$$
$$\left.\cdot\left[e^{-2\Gamma_{3n}(D_4-D_3)}-\rho_{3n}\right]+\rho_{4n}\left[\rho_{3n}e^{-2\Gamma_{2n}(D_4-D_3)}-1\right]\right\}), \quad (A20)$$

$$S_{3n} = \frac{1}{H}\left\{\frac{I}{2\Gamma_{3n}}e^{\Gamma_{4n}(D_5-D_4)}\left[x_{3n}e^{-\Gamma_{3n}(D_4-D_3)} + e^{\Gamma_{3n}(D_4-D_3)}\right]\right.$$
$$+\frac{J}{2\Gamma_{3n}}(\rho_{4n} + 1)e^{\Gamma_{4n}(D_5-D_4)}$$
$$\left.\cdot\left[y_{3n}e^{-\Gamma_{3n}(D_4-D_3)} - e^{-\Gamma_{3n}(D_4-D_3)}\right]\right\}, \quad (A21)$$

$$P_{2n} = \frac{2\mu_2}{G}\left(\mu_4\gamma_n + \Gamma_{4n}\right)\left(\frac{\mu_3\Gamma_{3n}}{\mu_4} + \Gamma_{4n}\right)(R_1 + R_2), \tag{A22}$$

$$Q_{2n} = (1/4H)(R_3 + R_4), \tag{A23}$$

$$R_{2n} = \frac{2\mu_2}{G}(\mu_4\gamma_n + \Gamma_{4n})\left(\frac{\mu_3\Gamma_{3n}}{\mu_4} + \Gamma_{4n}\right)e^{-\Gamma_{1n}(D_2 - D_1)}(S_1 + S_2), \tag{A24}$$

$$S_{2n} = (1/4H)(S_3 + S_4), \tag{A25}$$

$$
\begin{aligned}
P_{1n} = \frac{1}{G}\Bigg\{ &\left(\mu_4\gamma_n + \Gamma_{4n}\right)\left(\frac{\mu_3\Gamma_{3n}}{\mu_4} + \Gamma_{4n}\right) \\
&\cdot R_1\left(\mu_1 + \frac{\mu_2\Gamma_{3n}}{\Gamma_{2n}}\xi_{1n}\right)\left[e^{-2\Gamma_{1n}(D_2 - D_1)} + \omega_{1n}\right] \\
&+ R_2\left(\mu_1 + \frac{\mu_2\Gamma_{3n}}{\Gamma_{2n}}\xi'_{1n}\right)\left[e^{-2\Gamma_{bn}(D_2 - D_1)} + \omega'_{1n}\right]\Bigg\}, \tag{A26}
\end{aligned}
$$

$$
\begin{aligned}
Q_{1n} = \frac{1}{H}\Bigg\{ &R_3\left(\frac{\mu_1}{2\mu_2} + \frac{\Gamma_{1n}}{2\Gamma_{2n}}\tau_{1n}\right)\left[e^{-\Gamma_{1n}(D_2 - D_1)} + e^{\Gamma_{1n}(D_2 - D_1)\tau_{1n}}\right] \\
&+ R_4\left(\frac{\mu_1}{2\mu_2} + \frac{\Gamma_{1n}}{2\Gamma_{2n}}\tau'_{1n}\right)\left[e^{-\Gamma_{1n}(D_2 - D_1)} + e^{\Gamma_{1n}(D_2 - D_1)\tau'_{1n}}\right]\Bigg\}, \tag{A27}
\end{aligned}
$$

$$
\begin{aligned}
R_{1n} = \frac{1}{G}\Bigg\{ &\frac{S_1}{2\Gamma_{1n}}\left(\mu_4\gamma_n + \Gamma_{4n}\right)\left(\frac{\mu_3\Gamma_{3n}}{\mu_4} + \Gamma_{4n}\right) \\
&\cdot\left(\mu_1 + \frac{\mu_3\Gamma_{3n}}{\mu_2}\xi_{1n}\right)\left[e^{-2\Gamma_{1n}(D_2 - D_1)} - \omega_{1n}\right] \\
&+ S_2\left(\mu_1 + \frac{\mu_3\Gamma_{3n}}{\mu_2}\xi'_{1n}\right)\left[e^{-2\Gamma_{1n}(D_2 - D_1)} - \omega'_{1n}\right]\Bigg\}, \tag{A28}
\end{aligned}
$$

$$
\begin{aligned}
S_{1n} = \frac{1}{4H}\Bigg\{ &S_3\left(\frac{\mu_1}{\mu_2} + \frac{\tau_{1n}\Gamma_{1n}}{\Gamma_{2n}}\right)\left[e^{-\Gamma_{1n}(D_2 - D_1)} + e^{\Gamma_{1n}(D_2 - D_1)}\tau_{1n}\right] \\
&+ S_4\left(\frac{\mu_1}{\mu_2} + \frac{\tau'_{1n}\Gamma_{1n}}{\Gamma_{2n}}\right)\left[e^{-\Gamma_{1n}(D_2 - D_1)} + e^{\Gamma_{1n}(D_2 - D_1)}\tau'_{1n}\right]\Bigg\}, \tag{A29}
\end{aligned}
$$

$$
\begin{aligned}
G = &(\mu_1\gamma_n + \Gamma_{1n})(\mu_4\gamma_n + \Gamma_{1n})\left(\frac{\mu_3}{\mu_4} + \frac{\delta_{32n}\Gamma_{4n}}{\Gamma_{3n}}\right)\left(\frac{\mu_2}{\mu_1} + \frac{\delta_{1n}\Gamma_{2n}}{\Gamma_{1n}}\right) \\
&\cdot\left[\rho_{43n}\rho_{4n} - e^{-2\Gamma_{4n}(D_5 - D_4)}\right]\left[\rho_{32n} + e^{-2\Gamma_{3n}(D_4 - D_3)}\right] \\
&\cdot\left[\rho_{21n} + e^{-2\Gamma_{2n}(D_3 - D_2)}\right]\left[1 + e^{-2\Gamma_{1n}(D_2 - D_1)}\rho_{1n}\right], \tag{A30}
\end{aligned}
$$

$$H = (\mu_4\gamma_{4n} + \Gamma_{4n})\left[\rho_{43n}\rho_{4n} - e^{-2\Gamma_{4n}(D_5 - D_4)}\right], \tag{A31}$$

$$I = \left[\mu_4\Gamma_{3n}\left(\rho_{43n} - 1\right) + \Gamma_{4n}(\mu_4/\mu_3)\left(\rho_{4n} + \mu_4\right)\right]^{-1}, \tag{A32}$$

$$J = \left[\mu_4\rho_{43n}\left(\frac{\mu_4^2\delta_{4n}\gamma_n}{2\mu_3} + \Gamma_{4n}\right) + \frac{\mu_4}{2}\Gamma_{3n}\rho_{43n}\left(\frac{\mu_4\delta_{4n}\gamma_n}{\Gamma_{4n}} + 1\right)\right]^{-1}, \tag{A33}$$

$$R_1 = e^{-\Gamma_{4n}(D_5-D_4)} \left[e^{-\Gamma_{3n}(D_4-D_3)} + \rho_{3n} \right]$$
$$\cdot \left(\frac{\mu_1}{\mu_2} + \frac{\delta'_{32}\Gamma_{2n}}{\Gamma_{3n}} \right) \left[e^{-2\Gamma_{2n}(D_3-D_2)} + \xi_{2n} \right], \tag{A34}$$

$$R_2 = \rho_{4n} \left[e^{-2\Gamma_{3n}(D_4-D_3)}\rho_{3n} + 1 \right]$$
$$\cdot \left(\frac{\mu_1}{\mu_2} + \frac{\delta'_{32n}\Gamma_{2n}}{\Gamma_{3n}} \right) \left[e^{-2\Gamma_{2n}(D_3-D_2)} + \xi'_{32n} \right], \tag{A35}$$

$$R_3 = I e^{-\Gamma_{4n}(D_5-D_4)} \left[e^{-\Gamma_{3n}(D_4-D_3)} + e^{\Gamma_{3n}(D_4-D_3)} \right] x_{3n}$$
$$\cdot \left(\frac{\mu_2 x_{2n}}{\mu_3} + \frac{\Gamma_{2n}}{\Gamma_{3n}} \right) \left[e^{-\Gamma_{2n}(D_3-D_2)} + e^{\Gamma_{2n}(D_3-D_2)}\tau_{2n} \right], \tag{A36}$$

$$R_4 = J\left(\rho_{4n}+1\right) e^{-\Gamma_{4n}(D_5-D_4)} \left[e^{-\Gamma_{3n}(D_4-D_3)} + e^{\Gamma_{3n}(D_4-D_3)} \right] y_{3n}$$
$$\cdot \left(\frac{\mu_2}{\mu_3} + \frac{\Gamma_{2n}y_{2n}}{\Gamma_{3n}} \right) \left[e^{-\Gamma_{2n}(D_3-D_2)} + e^{\Gamma_{2n}(D_3-D_2)}\tau'_{2n} \right], \tag{A37}$$

$$S_1 = e^{-2\Gamma_{4n}(D_5-D_4)} \left[e^{-2\Gamma_{3n}(D_4-D_3)} + \rho_{3n} \right]$$
$$\cdot \left(\frac{\mu_1}{\mu_2} + \frac{\delta_{32n}\Gamma_{2n}}{\Gamma_{3n}} \right) \left[e^{-\Gamma_{2n}(D_3-D_2)} + \xi_{2n} \right], \tag{A38}$$

$$S_2 = \rho_{4n} \left[e^{-2\Gamma_{3n}(D_4-D_3)}\rho_{3n} + 1 \right]$$
$$\cdot \left(\frac{\mu_2}{\mu_3} + \frac{\delta'_{32n}\Gamma_{2n}}{\Gamma_{3n}} \right) \left[e^{-2\Gamma_{2n}(D_3-D_2)} - \xi'_{32n} \right], \tag{A39}$$

$$S_3 = (I/\Gamma_{2n})e^{-\Gamma_{4n}(D_5-D_4)} \left[x_{3n}e^{-\Gamma_{3n}(D_4-D_3)} + e^{\Gamma_{3n}(D_4-D_3)} \right]$$
$$\cdot \left(\frac{\mu_2 x_{2n}}{\mu_3} + \frac{\Gamma_{4n}}{\Gamma_{3n}} \right) \left[e^{-\Gamma_{2n}(D_3-D_2)} - e^{\Gamma_{2n}(D_3-D_2)}\tau_{2n} \right], \tag{A40}$$

$$S_4 = (J/\Gamma_{2n})\left(\rho_{4n}+1\right) e^{\Gamma_{4n}(D_5-D_4)} \left[y_{3n}e^{-\Gamma_{3n}(D_4-D_3)} + e^{\Gamma_{3n}(D_4-D_3)} \right]$$
$$\cdot \left(\frac{\mu_2}{\mu_3} + \frac{\Gamma_{4n}y_{2n}}{\Gamma_{3n}} \right) \left[e^{-\Gamma_{2n}(D_3-D_2)} - e^{\Gamma_{2n}(D_3-D_2)}\tau'_{2n} \right], \tag{A41}$$

$$x_{3n} = \frac{\mu_3\mu_4\Gamma_{4n}(\rho_{43n}-1) - \mu_4\Gamma_{3n}(\rho_{4n}+\mu_4)}{\mu_3\mu_4\Gamma_{4n}(\rho_{43n}-1) + \mu_4\Gamma_{3n}(\rho_{4n}+\mu_4)}, \tag{A42}$$

$$y_{3n} = \frac{\mu_4\rho_{43n}(\gamma_n\mu_4^2\delta_{4n}/\mu_3+2\Gamma_{4n}) - \mu_4\Gamma_{3n}\rho_{43n}(\gamma_n\mu_4\delta_{4n}/\Gamma_{4n}+1)}{\mu_4\rho_{43n}(\gamma_n\mu_4^2\delta_{4n}/\mu_3+2\Gamma_{4n}) + \mu_4\Gamma_{3n}\rho_{43n}(\gamma_n\mu_4\delta_{4n}/\Gamma_{4n}+1)}, \tag{A43}$$

$$x_{2n} = \frac{x_{3n}e^{-\Gamma_{3n}(D_4-D_3)} - e^{-\Gamma_{3n}(D_4-D_3)}}{x_{3n}e^{-\Gamma_{3n}(D_4-D_3)} + e^{-\Gamma_{3n}(D_4-D_3)}}, \tag{A44}$$

$$y_{2n} = \frac{y_{3n}e^{-\Gamma_{3n}(D_4-D_3)} - e^{-\Gamma_{3n}(D_4-D_3)}}{y_{3n}e^{-\Gamma_{3n}(D_4-D_3)} + e^{-\Gamma_{3n}(D_4-D_3)}}, \tag{A45}$$

$$\rho_{43n} = \frac{\mu_3\Gamma_{3n} - \delta_{32n}\mu_4\Gamma_{4n}}{\mu_3\Gamma_{3n} + \delta_{32n}\mu_4\Gamma_{4n}}, \ \rho_{32n} = \frac{\mu_3\Gamma_{2n} - \delta_{21n}\mu_2\Gamma_{3n}}{\mu_3\Gamma_{2n} + \delta_{21n}\mu_2\Gamma_{3n}}, \quad \text{(A46)}$$

$$\rho_{21n} = \frac{\mu_1\Gamma_{1n} - \delta_{21n}\mu_2\Gamma_{2n}}{\mu_1\Gamma_{1n} + \delta_{21n}\mu_2\Gamma_{2n}}, \ \rho_{4n} = \frac{\mu_4\gamma_n - \Gamma_{4n}}{\mu_4\gamma_n + \Gamma_{4n}}, \quad \text{(A47)}$$

$$\rho_{3n} = \frac{\mu_4\Gamma_{4n} - \mu_3\Gamma_{3n}}{\mu_4\Gamma_{4n} + \mu_3\Gamma_{3n}}, \ \rho_{1n} = \frac{\mu_1\gamma_n - \Gamma_{1n}}{\mu_1\gamma_n + \Gamma_{1n}}, \quad \text{(A48)}$$

$$\delta_{32n} = \frac{e^{-2\Gamma_{3n}(D_4-D_3)} - \rho_{32n}}{e^{-2\Gamma_{3n}(D_4-D_3)} + \rho_{32n}}, \ \delta_{21n} = \frac{e^{-2\Gamma_{2n}(D_3-D_2)} - \rho_{21n}}{e^{-2\Gamma_{2n}(D_3-D_2)} + \rho_{21n}}, \quad \text{(A49)}$$

$$\delta_{1n} = \frac{e^{-2\Gamma_{1n}(D_2-D_1)} - \rho_{1n}}{e^{-2\Gamma_{1n}(D_2-D_1)} + \rho_{1n}}, \ \delta'_{32n} = \frac{e^{-2\Gamma_{3n}(D_3-D_2)}\rho_{3n} - 1}{e^{-2\Gamma_{3n}(D_4-D_3)}\rho_{3n} + 1}, \quad \text{(A50)}$$

$$\delta_{4n} = (\rho_{4n} - 1)/(\rho_{4n} + 1), \quad \text{(A51)}$$

$$\xi_{2n} = \frac{\mu_2\Gamma_{3n} - \mu_3\delta_{32n}\Gamma_{2n}}{\mu_2\Gamma_{3n} + \mu_3\delta_{32n}\Gamma_{2n}}, \quad \xi'_{2n} = \frac{\mu_2\Gamma_{3n} - \mu_3\delta'_{32n}\Gamma_{2n}}{\mu_2\Gamma_{3n} + \mu_3\delta'_{32n}\Gamma_{2n}}, \quad \text{(A52)}$$

$$\xi_{1n} = \frac{e^{-2\Gamma_{2n}(D_3-D_2)} - \xi_{2n}}{e^{-2\Gamma_{2n}(D_3-D_2)} + \xi_{2n}}, \quad \xi'_{1n} = \frac{e^{-2\Gamma_{2n}(D_3-D_2)} - \xi'_{2n}}{e^{-2\Gamma_{2n}(D_3-D_2)} + \xi'_{2n}}, \quad \text{(A53)}$$

$$\tau_{2n} = \frac{\mu_2 x_{2n}\Gamma_{3n} - \mu_3\Gamma_{2n}}{\mu_2 x_{2n}\Gamma_{3n} + \mu_3\Gamma_{2n}}, \quad \tau'_{2n} = \frac{\mu_2\Gamma_{3n} - \mu_3 y_{2n}\Gamma_{2n}}{\mu_2\Gamma_{3n} + \mu_3 y_{2n}\Gamma_{2n}}, \quad \text{(A54)}$$

$$\tau_{1n} = \frac{e^{-\Gamma_{2n}(D_3-D_2)} - e^{-2\Gamma_{2n}(D_3-D_2)}\tau_{2n}}{e^{-\Gamma_{2n}(D_3-D_2)} + e^{-2\Gamma_{2n}(D_3-D_2)}\tau_{2n}}$$

$$\tau'_{1n} = \frac{e^{-\Gamma_{2n}(D_3-D_2)} - e^{-2\Gamma_{2n}(D_3-D_2)}\tau'_{2n}}{e^{-\Gamma_{2n}(D_3-D_2)} + e^{-2\Gamma_{2n}(D_3-D_2)}\tau'_{2n}}, \quad \text{(A55)}$$

$$\omega_{1n} = \frac{\mu_1\Gamma_{2n} - \mu_2\xi_{1n}\Gamma_{3n}}{\mu_1\Gamma_{2n} + \mu_2\xi_{1n}\Gamma_{3n}}, \quad \omega'_{1n} = \frac{\mu_1\Gamma_{2n} - \mu_2\xi'_{1n}\Gamma_{3n}}{\mu_1\Gamma_{2n} + \mu_2\xi'_{1n}\Gamma_{3n}}. \quad \text{(A56)}$$

Equations (A4)–(A9) with (A10)–(A56) can be used in Section 4 to solve the Wiener-Hopf equations (53) and (54) to obtain the formal solution.

REFERENCES

1. Knott, E. F., J. F. Shaeffer, and M. T. Tuley, *Radar Cross Section: Its Prediction, Measurement and Reduction*, Artech House, Boston, 1985.
2. Lee, S.-W. and H. Ling, "Data book for cavity RCS: Version 1," *Tech. Rep.*, No. SWL89-1, Univ. Illinois, Urbana, 1989.
3. Lee, S.-W. and R. J. Marhefka, "Data book of high-frequency RCS: Version 2," *Tech. Rep.*, Univ. Illinois, Urbana, 1989.

4. Stone, W. R. (ed.), *Radar Cross Sections of Complex Objects*, IEEE Press, New York, 1990.

5. Bhattacharyya, A. K. and D. L. Sengupta, *Radar Cross Section Analysis and Control*, Artech House, Boston, 1991.

6. Bernard, J. M. L., G. Pelosi, and P. Ya. Ufimtsev (eds.), *Special Issue on Radar Cross Section of Complex Objects, Ann. Telecommun.*, Vol. 50, No. 5–6, 1995.

7. Lee, C. S. and S.-W. Lee, "RCS of coated circular waveguide terminated by a perfect conductor," *IEEE Trans. Antennas Propagat.*, Vol. 35, No. 4, 391–398, 1987.

8. Altintaş, A., P. H. Pathak, and M. C. Liang, "A selective modal scheme for the analysis of EM coupling into or radiation from large open-ended waveguides," *IEEE Trans. Antennas Propagat.*, Vol. 36, No. 1, 84–96, 1988.

9. Ling, H., R.-C. Chou, and S.-W. Lee, "Shooting and bouncing rays: Calculating the RCS of an arbitrary shaped cavity," *IEEE Trans. Antennas Propagat.*, Vol. 37, No. 2, 194–205, 1989.

10. Pathak, P. H. and R. J. Burkholder, "Modal, ray, and beam techniques for analyzing the EM scattering by open-ended waveguide cavities," *IEEE Trans. Antennas Propagat.*, Vol. 37, No. 5, 635–647, 1989.

11. Pathak, P. H. and R. J. Burkholder, "A reciprocity formulation for the EM scattering by an obstacle within a large open cavity," *IEEE Trans. Microwave Theory Tech.*, Vol. 41, No. 4, 702–707, 1993.

12. Lee, R. and T.-T. Chia, "Analysis of electromagnetic scattering from a cavity with a complex termination by means of a hybrid ray-FDTD method," *IEEE Trans. Antennas Propagat.*, Vol. 41, No. 11, 1560–1569, 1993.

13. Ohnuki, S. and T. Hinata, "Radar cross section of an open-ended rectangular cylinder with an iris inside the cavity," *IEICE Trans. Electron.*, Vol. E81-C, No. 12, 1875–1880, 1998.

14. Noble, B., *Methods Based on the Wiener-Hopf Technique for the Solution of Partial Differential Equations*, Pergamon, London, 1958.

15. Mittra, R. and S.-W. Lee, *Analytical Techniques in the Theory of Guided Waves, Macmillan*, New York, 1971.

16. Kobayashi, K., "Wiener-Hopf and modified residue calculus techniques," *Analysis Methods for Electromagnetic Wave Problems*, E. Yamashita (ed.), Chap. 8, Artech House, Boston, 1990.

17. Büyükaksoy, A., F. Birbir, and E. Erdoğan, "Scattering

characteristics of a rectangular groove in a reactive surface," *IEEE Trans. Antennas and Propagat.*, Vol. 43, No. 12, 1450–1458, 1995.

18. Çetiner, B. A., A. Büyükaksoy, and F. Güneş, "Diffraction of electromagnetic waves by an open ended parallel plate waveguide cavity with impedance walls," *Progress In Electromagnetics Research*, PIER 26, 165–197, 2000.

19. Kobayashi, K. and A. Sawai, "Plane wave diffraction by an open-ended parallel plate waveguide cavity," *Journal of Electromagnetic Waves and Applications*, Vol. 6, No. 4, 475–512, 1992.

20. Kobayashi, K., S. Koshikawa, and A. Sawai, "Diffraction by a parallel-plate waveguide cavity with dielectric/ferrite loading: Part 1 — The case of E polarization," *Progress In Electromagnetics Research*, PIER 8, 377–426, 1994.

21. Koshikawa, S. and K. Kobayashi, "Diffraction by a parallel-plate waveguide cavity with dielectric/ferrite loading: Part 2 — The case of H polarization," *Progress In Electromagnetics Research*, PIER 8, 427–458, 1994.

22. Koshikawa, S., T. Momose, and K. Kobayashi, "RCS of a parallel-plate waveguide cavity with three-layer material loading," *IEICE Trans. Electron.*, Vol. E77-C, No. 9, 1514–1521, 1994.

23. Koshikawa, S. and K. Kobayashi, "Diffraction by a terminated, semi-infinite parallel-plate waveguide with three-layer material loading," *IEEE Trans. Antennas and Propagat.*, Vol. 45, No. 6, 949–959, 1997.

24. Okada, S., S. Koshikawa, and K. Kobayashi, "Wiener-Hopf analysis of the plane wave diffraction by a finite parallel-plate waveguide with three-layer material loading: Part 1 — The case of E polarization," *Telecommunications and Radio Engineering*, Vol. 58, No. 1 & 2, 53–65, 2002.

25. Okada, S., S. Koshikawa, and K. Kobayashi, "Wiener-Hopf analysis of the plane wave diffraction by a finite parallel-plate waveguide with three-layer material loading: Part 2 — The case of H polarization," *Telecommunications and Radio Engineering*, Vol. 58, No. 1 & 2, 66–75, 2002.

26. Shang, E. H. and K. Kobayashi, "Plane wave diffraction by a finite parallel-plate waveguide with four-layer material loading: Part II — The case of H polarization," *Progress In Electromagnetics Research B*, Vol. 6, 267–294, 2008.

27. Kobayashi, K., "On generalized gamma functions occurring in diffraction theory," *J. Phys. Soc. Japan*, Vol. 60, No. 5, 1501–1512, 1991.